UNIVERSITY OF BIRMINGHAM

Investigating whether suppressing the DNA damage response is neuroprotective in *Drosophila* models of C9orf72 ALS-FTD

By Lauren Butler
ID: [redacted]

A thesis submitted to the University of Birmingham for the degree of MSc by Research Cancer and Genomic Sciences

Institute of Cancer and Genomic Sciences
College of Medical and Dental Sciences
University of Birmingham
September 2023

Abstract

Amyotrophic lateral sclerosis (ALS) and frontotemporal dementia (FTD) are neurodegenerative diseases that have a clear genetic overlap. The most common cause of both is a hexanucleotide repeat expansion in the C9orf72 gene. This has the ability to cause genomic instability and DNA damage. DNA damage is a key feature of many neurodegenerative diseases. Accumulation of double strand DNA breaks leads to chronic activation of the DNA damage response (DDR) and neurodegeneration. Previous work has shown that inhibiting DDR proteins, including ataxia-telangiectasia-mutated kinase (ATM) and checkpoint kinase 2 (Chk2), in a *Drosophila* Alzheimer's disease model was neuroprotective. In this project I investigated whether similar knockdown of DDR proteins would also be neuroprotective in a *Drosophila* ALS-FTD model. I have shown that knockdown of ATM improved the survival rate of my *Drosophila* ALS-FTD model but produced inconsistent results on its effect on the motor function decline. Repetition of the motor function experiments would be required to give a definitive result.

Acknowledgements

I would like to thank my supervisor Dr Richard Tuxworth for giving me the opportunity to undertake this project, and for all the support and guidance he has given me. I would like to additionally thank him for inviting me to present the research in this project at Neurofly 2022, an experience I truly enjoyed and am very grateful for.

I would also like to thank Matt Taylor and Charlie George for their guidance as colleagues and friends throughout this project. Thank you to Laura Hawkins for the coffee and cake trips which kept me sane!

Contents

List of Figures

List of Tables

Table of Abbreviations

AD	Alzheimer's disease
ALS	amyotrophic lateral sclerosis
ATM	ataxia telangiectasia mutated kinase
ATR	ATM and Rad3-related kinase
BER	base excision repair
bvFTD	behavioural variant frontotemporal dementia
C9orf72	Chromosome 9 open reading frame 72
DDR	DNA damage response
DNA-PK	DNA-dependant protein kinase
DPRs	dipeptide repeat proteins
FTD	frontotemporal dementia
FUS	fused in sarcoma
gDNA	genomic DNA
GEF	guanine exchange factor
GFP	green fluorescent protein
GG-NER	global genome NER
GRN	Granulin precursor
HD	Huntington's disease
HR	homologous recombination
HRE	hexanucleotide repeat expansion
iMNs	induced motor neurons
iPSCs	induced pluripotent stem cells
KD	knockdown
LSM	laser scanning microscope
MAPT	Microtubule associated protein tau
MMR	mismatch repair

MRN	Mre11, Rad50 and NBS1 complex
NCT	nucleocytoplasmic transport
NER	nucleotide excision repair
NHEJ	non-homologous end-joining
PBS	phosphate buffered saline
PD	Parkinson’s disease
PIKKs	phosphatidylinositol-3-kinase-like kinase family
PPA	primary progressive aphasia
RAN translation	repeat associated non-ATG translation
RBPs	RNA binding proteins
RNAi	RNA interference
ROS	reactive oxygen species
RT	room temperature
shRNA	short hairpin RNA
SOD1	Superoxide dismutase 1
SSBR	single strand break repair
ssDNA	single strand DNA
svFTD	semantic variant FTD
TARDBP	TAR DNA binding protein
TC-NER	transcription-coupled NER
TDP-43	TAR DNA-binding protein 43
VNC	ventral nerve cord

1. Introduction

1.1. ALS-FTD: A spectrum

Amyotrophic lateral sclerosis (ALS) is an adult-onset neurodegenerative disease. It is characterised by the progressive loss of motor function due to the deterioration of motor neurons in the frontal cortex, brainstem, and spinal cord. The result of this presents initially as muscle weakness and spasticity, progressing to full paralysis of limbs and muscles required for speech, and fatally the denervation of respiratory muscles (Cleveland and Rothstein, 2001). With an incidence rate of 2 per 100,000 (Yoshida et al, 1886), the average life expectancy from diagnosis is 3-5 years (Robberecht and Philips, 2013). This is shorter, around 2 years, in patients who also develop frontotemporal dementia (FTD) (Ferrari et al, 2011).

FTD is second only to Alzheimer's disease as a cause of dementia, accounting for 10% of all dementias. It can be separated into two main presentations; the behavioural variant (bvFTD), which presents as cognitive and behavioural changes, and primary progressive aphasia (PPA), which can be further categorised as non-fluent aphasia (nfPPA) and semantic variant (svFTD). PPA displays primarily as language deficits (Goldman and Van Deerlin, 2018). Pathologically, FTD is associated with atrophy and spongiform morphology of the frontal and anterior temporal lobes (Bahia and Takada, 2013).

The overlap between these two disorders was first reported in 1981 when AJ Hudson identified 26 sporadic ALS cases that were associated with dementia, as well 10 familial ALS cases which all displayed frontal and frontotemporal degeneration in addition to typical ALS neuropathology (Hudson, 1981). It is now understood that 50% of ALS patients develop

traits of FTD, most commonly bvFTD, whilst 30% of FTD patients will develop motor dysfunction indicative of ALS (Burrell et al, 2011; Abramzon et al, 2022). The overlapping clinical and neuropathological features gives reason to suggest that these diseases share neurodegenerative pathways and form opposite ends of a disease spectrum.

1.2. Pathogenesis of ALS-FTD

Although the majority of cases are sporadic for both ALS and FTD, familial forms make up 10% and 40% of ALS and FTD respectively (Ferrari et al, 2011; Abramzon et al, 2022). Considerable efforts in identifying the genetics implicated in the pathology of ALS and FTD has revealed a clear overlap in the associated genes and pathological characteristics, supporting the idea these neurodegenerative conditions form a neurodegenerative spectrum, illustrated in Figure 1.

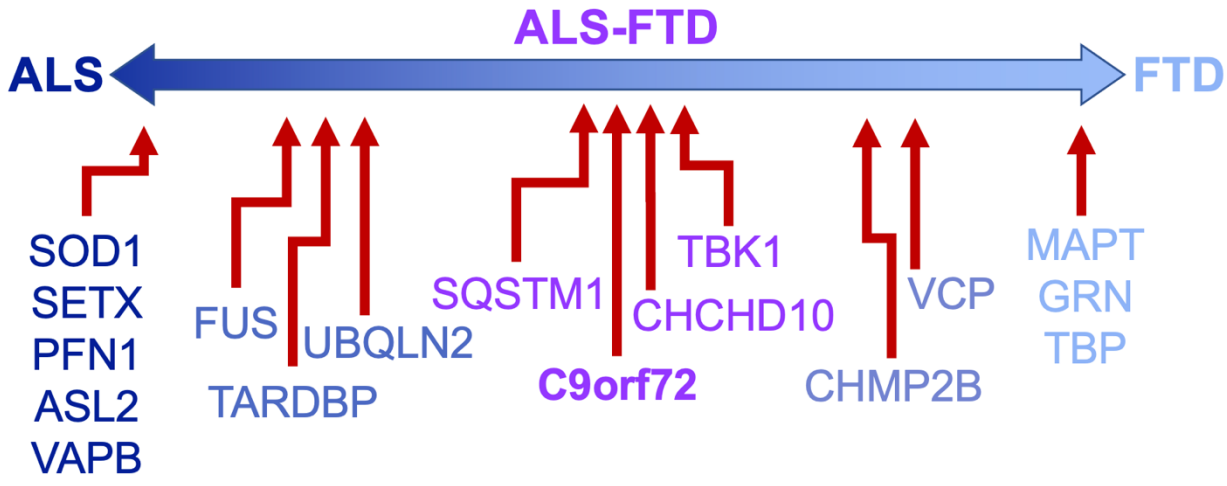

Figure 1: A Schematic of the ALS-FTD Neurodegenerative Spectrum
Common causative genes of ALS and FTD are shown, with 'pure' ALS and FTD genes at either end of the spectrum such as SOD1 and MAPT. Genes more predominantly causative of ALS, but FTD can be present, are towards the left of the spectrum such as FUS and TARDBP. Similarly, FTD genes that sometimes present with ALS sit towards the right side. C9orf72 sits central of the spectrum as the most common cause of ALS-FTD. Figure made with information from Meizini et al, 2019, and Ranganathan et al, 2015.

1.2.1. ALS-associated genetics

Whilst there are large number of genes identified to be causative or disease-modifying of ALS, the most frequently occurring pathogenic mutants are found in the Superoxide dismutase 1 (SOD1), Chromosome 9 open reading frame 72 (C9orf72), TAR-DNA binding protein (TARDBP), and fused in sarcoma (FUS) genes (Mejzini et al, 2019).

SOD1 was the first gene to be implicated in ALS pathology in 1993 (Rosen et al, 1993), and causes 20% of familial ALS and 2% of sporadic ALS (Marangi and Traynor, 2015). Located on chromosome 21q22.11, it is a 153-amino acid cytoplasmic homodimer, which binds copper and zinc ions and catalyses the production of oxygen and hydrogen peroxide from superoxide produced during oxidative phosphorylation (Cleveland et al, 2001). There are over 185 reported pathogenic mutants of SOD1, the majority of which are missense mutations and vary in phenotypes and severity (Meizini et al, 2019). SOD1 mutants exert toxicity through toxic gain of function mechanisms. They are able to cause oxidative stress by binding to Rac1, chronically activating Nox2 and leading to the overproduction of superoxide. SOD1 mutants also interact with Derlin-1 in the cytosol. This inhibits ER-associated degradation of misfolded proteins causing a state of ER stress and elicits apoptosis (Hayashi and Homma, 2016). Other mechanisms of toxicity of SOD1 mutants such as excitotoxicity, mitochondrial dysfunction and axonal transport dysfunction are reviewed by Hayashi and Homma (2016).

TARDBP mutations make up 4% of familial ALS and 1% of sporadic ALS cases (Marangi and Traynor, 2015). Located on chromosome 1p36.22, it encodes the TAR DNA-binding protein 43 (TDP-43) which plays significant roles in RNA processing, such as transcription, splicing, transport, and maintaining RNA stability. TDP-43 is normally located in the nucleus

but does have the ability to move back and forth between the nucleus and cytoplasm (Meizini et al, 2019). 48 mutations in TARDBP have been associated with ALS, many of which cause irregular RNA processing such as defective splicing, dysregulated expression of other proteins, and mRNA instability (Meizini et al, 2019; Ranganathan et al, 2020). What appears to be the most notable consequence of pathogenic TARDBP mutations is the movement of TDP-43 from the nucleus to the cytoplasm and it's accelerated aggregation (Johnson et al, 2009). Ubiquitinated aggregations of TDP-43 have been identified in the cytoplasm of neurons in 97% of ALS patients, both familial and sporadic cases, (Ranganathan et al, 2020) as well as cases that are absent of pathogenic mutations in the TARDBP gene but do contain the pathogenic expansion in the C9orf72 gene (Meizini et al, 2019). These aggregates have been proposed to cause both loss of function from the depleted nuclear TDP-43, and gain of function due to the toxic nature of the inclusions, and it is clear that they have a significant role in the pathogenesis of ALS (Abramzon et al, 2020).

Functionally homologous to TDP-43 is fused in sarcoma (FUS). Mutations in the FUS gene, located on chromosome 16p11.2, also account for 4% of familial ALS and 1% of sporadic ALS (Ranganathan et al, 2020). Much like TDP-43, FUS is an RNA binding protein which is involved in transcription, pre-mRNA splicing, and RNA transport, however it also plays a role in homologous recombination and non-homologous end joining in DNA repair (Meizini et al, 2019). Due to the FUS protein's prion-like domain, and its ability for nucleocytoplasmic transport (NCT), mutations in FUS are also able to cause aggregations of the protein in the cytoplasm, with FUS-positive aggregates having been identified in the brains and spinal cords of ALS patients with FUS mutants (Robberecht and Philips, 2013). These aggregates propose similar loss of function and gain of function as TDP-43 aggregates, with mis-localisation of FUS impacting RNA processing, and FUS aggregates propagating through neuronal tissues in a prion-like manner (Abramzon et al, 2020).

1.2.2. FTD-associated genetics

TDP-43 and FUS proteinopathies are not only prevalent in ALS, they are two of the three proteinopathies present in FTD also, the third being the tau protein. TDP-43 pathology underlies 50% of FTD, with tau and FUS underlying 40% and 10% respectively (Goldman and Van Deerlin, 2018). With 40% of FTD cases being familial and predominantly autosomal dominant, there is a close correlation between the mutated genes and associated neuropathology. In rare cases, TARDBP and FUS mutations are found in FTD, however there are three genes responsible for the majority of autosomal dominant cases of FTD; microtubule associated protein tau (MAPT), granulin precursor (GRN) and C9orf72 (Sieben et al, 2012; Goldman and Van Deerlin, 2018).

MAPT is the gene which encodes the tau protein, with mutations found in 5% of all FTD cases, and making up 10-20% of autosomal dominant cases. It is therefore evident that tau pathology is present in all cases of FTD with mutated MAPT (Bahia and Takada, 2013; Goldman and Van Deerlin, 2018). Under normal physiological conditions, Tau, a microtubule-associated protein, is essential for maintaining the stability of neuronal microtubules. MAPT mutations alter the tau proteins isoform ratios and binding ability to microtubules, leading to hyperphosphorylated tau filaments accumulating in neuronal and glial cells creating the identifiable neuropathology of FTD (Bahia and Takada, 2013). So far, MAPT mutations are associated with FTD only and have not been found in any cases that also present with ALS (Goldman and Van Deerlin, 2018).

GRN and C9orf72 have both been identified to be causative of FTD with TDP-43 pathology. GRN encodes the growth factor precursor progranulin, and mutations in the gene have been

shown to account for around 20% of familial cases and 5% of sporadic FTD cases (Mackenzie, Rademakers and Neumann, 2010). However, despite its prominent occurrence in FTD, GRN mutations have not been implicated in ALS, much like MAPT mutations (Goldman and Van Deerlin, 2018).

C9orf72 mutations are the most common cause of both ALS, FTD, and ALS-FTD. They are found in 40% of familial ALS cases, and around 25% of familial FTD cases, but almost 90% of cases that present with symptoms of both diseases (Goldman and Van Deerlin, 2018; Ranganathan et al, 2020). In C9orf72-related cases of both ALS and FTD, neuronal inclusions are typically TDP-43 positive, establishing further genetic and histological links between the two diseases, however the mechanism of pathogenicity for this mutation is still debated (Bennion and Pickering-Brown, 2014).

1.3. C9orf72 mechanisms of disease

The C9orf72 mutation is a hexanucleotide repeat expansion (HRE) of the sequence GGGGCC (G_4C_2) which was discovered in 2011 (DeJesus-Hernandez et al, 2011; Renton et al, 2011). Located at ch9p21, the hexanucleotide repeat is found within intron 1 of chromosome 9 open reading frame 72 (C9orf72), between two transcription initiation sites (Ranganathan et al, 2020). The gene (illustrated in figure 2) produces three alternatively spliced transcripts which are translated into two different protein isoforms. The hexanucleotide repeat is within intron 1 in variants 1 and 3, but is within the promoter region of variant 2 and so is not included in the pre-mRNA (Balendra and Isaacs, 2018). Variant 1 encodes a short, 222-amino-acid protein isoform of exons 2-5, whilst variants 2 and 3 encode a long, 481-amino-acid isoform of exons 2-11 (Smeyers, Banchi and Latouche, 2021). In non-carriers of the C9orf72 mutation, the G_4C_2 sequence usually has under 10

repeats, with most studies considering the pathological threshold to be 30 repeats. However, in ALS and FTD patients, expansions consisting of hundreds or thousands of repeats are more commonly observed although this can be hard to determine exactly due to somatic instability (Balendra and Isaacs, 2018).

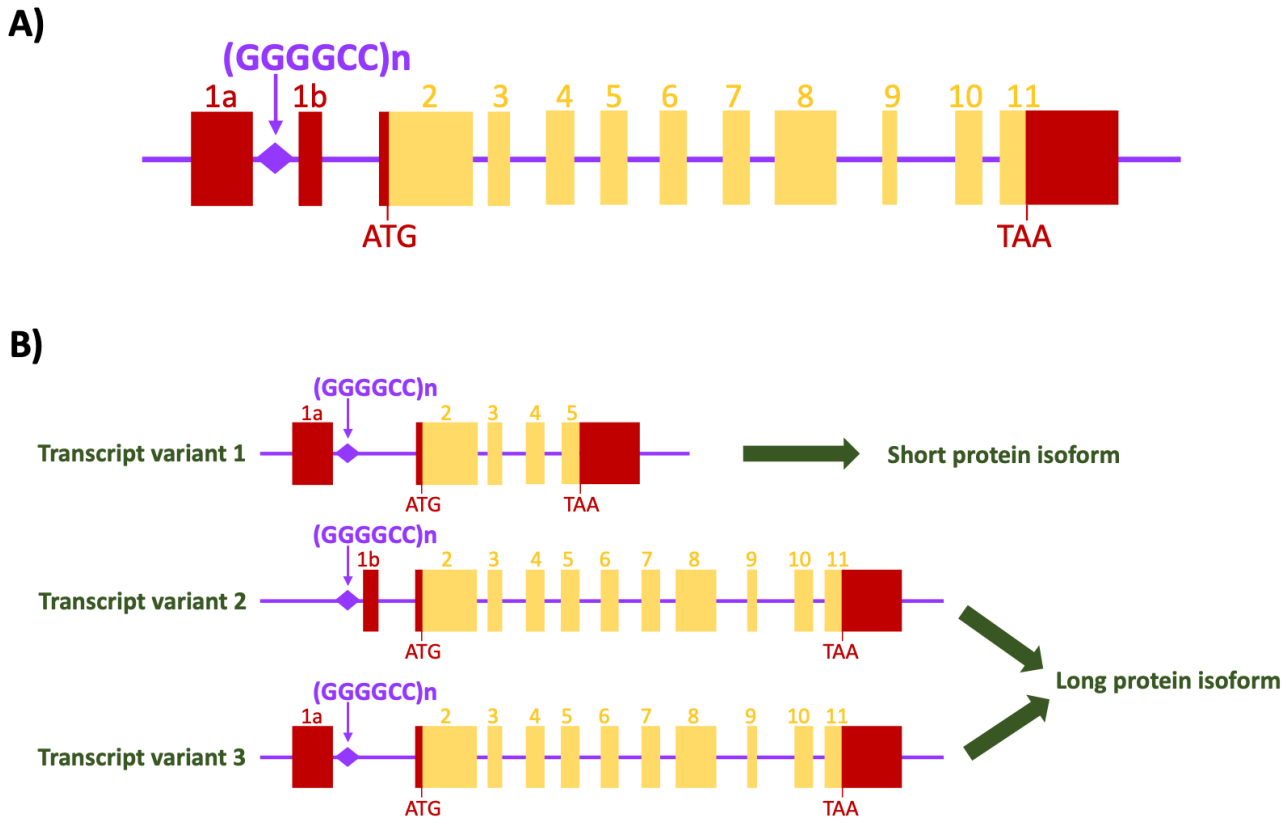

Figure 2: C9orf72 gene structure
(A) The C9orf72 gene contains 2 non-coding exons, 1a and 1b (shown in red), and 10 coding exons, 2-11 (shown in yellow). The G_4C_2 expansion is located in intron 1, between the two non-coding exons 1a and 1b. (B) The gene produces three alternatively spliced transcripts, which produce two different protein isoforms, the short isoform and the long isoform. Figure not to scale. Adapted from Balendra and Isaacs (2018).

The C9orf72 protein is expressed in the brain, spinal cord, and immune system, with studies showing that it is localised to presynapses, and is predominantly identified as the long isoform (Frick et al, 2018; Smeyers, Banchi and Latouche, 2021). Having found to contain DENN (differentially expressed in normal and neoplastic cells) domains, it is believed that the C9orf72 protein acts as a guanine exchange factor (GEF) for Rab GTPases (Robberecht

and Philips, 2013; Ranganathan et al, 2020; Frick et al, 2018). Several studies have demonstrated that C9orf72 protein's GEF activity modulates neurotransmission, endosomal and autophagosomal functions. By forming a complex with SMRC8 and WDR41, it acts as a GEF for Rab8A and Rab39B, controlling vesicle trafficking and autophagic flux, as well as interacting with the Rab3 protein family, which are found in synaptic vesicles and are involved in neurotransmitter release (Sellier et al, 2016; Frick et al, 2018). The C9orf72 protein has also been found to interact with the Rab1a and ULK1 autophagy initiation complex, where it regulates the trafficking of the ULK1 complex to the phagophore thereby controlling the initiation of autophagy (Webster et al, 2016).

The growing knowledge of the physiological functions of the C9orf72 protein is crucial to the understanding of how the HRE contributes to neurodegeneration. So far, there is evidence for three different mechanisms of pathogenicity; a loss of function effect as result of C9orf72 haploinsufficiency, and two gain of function effects from accumulated RNA foci, and dipeptide repeat proteins (DPRs) generated from the expansion.

1.3.1. C9orf72 protein haploinsufficiency

The possible loss of function of the C9orf72 protein as a disease-driving mechanism has arisen from studies recording reduced transcript variants in the frontal cortex, the cerebellum, the motor cortex, the cervical spinal cord, blood lymphocytes and induced pluripotent stem cells (iPSCs)-derived neurons of C9orf72 related ALS-FTD patients. In some cases, the mRNA levels were reduced by up to 50% (DeJesus-Hernandez et al, 2011; Balendra and Isaacs, 2018). Given C9orf72's proposed role of initiating and controlling autophagic flux, depleted C9orf72 expression has been found to impair autophagy (Balendra and Isaacs, 2018). Evidence to support the impairment of autophagy relates

specifically to its initiation rather than late stages of degradation and suggests that C9orf72 is more important to the formation of the autophagosome rather than degradation by the lysosome (Sellier et al, 2016). Impaired autophagy leads to the accumulation of cytoplasmic aggregates unable to be sequestered by the autophagosome, such as TDP-43 and p62 thereby creating two of the histopathological hallmarks of ALS-FTD, as well as the inability to clear accumulated DPRs (Sellier et al, 2016; Shi et al, 2018).

Autophagy is an important component in maintaining homeostatic synaptic plasticity in cortical neurons in response to chronic glutamate signalling. It is plausible to suggest that impaired autophagy from the reduced C9orf72 activity may be the cause of elevated glutamate receptor levels that have been found in the spinal cord and cortical tissue of C9orf72-related ALS-FTD patients (Balendra and Isaacs, 2018; Shi et al, 2018). Elevated NMDA (NR1) and AMPA (GLUR1) receptor levels were reported in induced motor neurons (iMNs) of C9orf72 ALS-FTD patients, leading to increased excitotoxicity (Shi et al, 2018). Glutamate accumulation in the cerebral spinal fluid of ALS patients has also been observed. This is believed to be caused by atypical splicing and dysfunction of the EAAT2 glutamate transporter and reduced glutamate uptake in astrocytes, induced by DPRs. The consequence of this is a further increase in excitotoxicity in neurons with elevated glutamate receptors, potentially triggering neurodegeneration (Shi et al, 2018).

However, many studies have failed to demonstrate that haploinsufficiency alone is sufficient to cause neurodegeneration (Koppers et al, 2015; Jiang et al, 2016), but rather that it may act in parallel with gain of function mechanisms to trigger disease.

1.3.2. RNA foci toxicity

The first of the gain of function mechanisms is toxicity from accumulated RNA foci. The HRE can be bidirectionally transcribed, producing both G_4C_2 sense and C_2G_4 anti-sense RNA transcripts. Post-mortem brain analysis found these sense and anti-sense foci in ~37% and 26% of frontal cortex neurons, respectively, as well as 25% and 18% of granule cell neurons in the hippocampus and 21% and 9% of granule cell neurons in the cerebellum (Mizeilinska et al, 2013). Another study produced similar findings, also showing that 70% of cerebellum perkinje cells contained HRE-retaining RNA foci (DeJesus-Hernandez et al, 2017).

These RNA foci are found in the form of secondary structures such as G-quadruplex, hairpin structures and R-loops made up of C9orf72 HRE-retaining DNA and RNA (Haeusler et al, 2014). Once in these structures, they have the ability to sequester RNA binding proteins (RBPs), rendering them unable to function. Several studies have tried to identify how many RBPs associate with the C9orf72 RNA foci, which a definitive answer has not yet been determined. One of the RBPs that has been identified is Nucleolin (NCL), which is essential for RNA processing, and has been found to be mis-localised in C9orf72 patient cells (Haeusler et al, 2014). The same study demonstrated that motor neurons containing the C9orf72 HRE have aborted transcription, defective RNA processing, and higher levels of nucleolar stress (Haeusler et al, 2014). Other RBPs found to be sequestered by C9orf72 foci include heterogeneous nuclear ribonucleoprotein A1 (hnRNPA1), serine/arginine-rich splicing factor 2 (SRSF2), PUR-α, and adenosine deaminase RNA specific B2 (ADARB2). These also play significant roles in RNA processing such as pre-mRNA splicing and mRNA translation which would likely be impacted if sequestered by the C9orf72 RNA foci (Ranganathan et al, 2020).

1.3.3. Dipeptide repeat protein toxicity

The sense and anti-sense RNA transcripts containing the C9orf72 HRE are able to be translated through non-canonical repeat associated non-ATG (RAN) translation, which occurs across the long hairpin forming G_4C_2 repeated sequence (Robberecht and Philips, 2013). Without the need for the AUG start codon, the repeated sequence is able to be translated in multiple reading frames, resulting in the generation of five different DPRs: Poly-glycine-alanine (GA), glycine-proline (GP), glycine-arginine (GR), proline-alanine (PA), and proline-arginine (PR) (Ranganathan et al, 2020). These DPRs aggregate to form cytoplasmic inclusions in neurons and glia, which have been shown to be p62-positive. They have been found in the neocortex, cerebellum, thalamus, and hippocampus, but are rarely seen in the brainstem and spinal cord (Balendra and Isaacs, 2018; Ranganathan et al, 2020).

Even though all five DPRs form inclusions, it is the arginine rich DPRs, poly-GR and Poly-PR, which are believed to be toxic and most likely to be responsible for inducing neurodegeneration (Mizielinska et al, 2014; Lopez-Gonzalez et al, 2016; Xu, W. and Xu, J., 2018). They have been shown to cause nucleolar stress through binding to the nucleolus, inducing the translocation of nucleophosmin, and disrupting ribosomal RNA synthesis, pre-mRNA splicing, mitochondrial function, NCT, and the formation of stress granules (Kwon et al, 2014; Tao et al, 2015; Moens, Partridge, and Isaacs, 2017). Xu, W. and Xu, J. (2018) have also demonstrated that arginine rich DPRs cause excitotoxicity. They showed that poly-GR and PR expression led to altered synaptic structures and promoted glutamate release, but only in *Drosophila* glutamatergic neurons. Meanwhile Kwon et al (2014) suggests that the Poly-PR protein is associated with aberrant splicing of EAAT2, all of which would cause excitotoxicity capable of causing neurodegeneration.

Poly-GA has also been shown to exert mild toxicity in a few studies (May et al, 2014; Zhang et al, 2014). Some of poly-GA's co-aggregating proteins have been identified, and whilst many are involved in the ubiquitin-proteasome system, inhibiting proteasome activity and causing ER stress (Zhang et al 2014), another that gets sequestered was Unc119. In poly-PA expressing neurons, soluble Unc119 levels were reduced, and when Unc119 was knocked down in hippocampal neurons to replicate the sequestration, it led to dendrite withering and induced neuronal death (May et al, 2014). However other studies such as Mizielinska et al, (2014) and Tao et al, (2015) observe no toxicity in poly-GA models so to what extent poly-PA contributes to neurodegeneration is still unknown.

The uncertainty around whether DPRs are the cause of C9orf72 neurodegeneration is often associated with the fact the DPRs localise to areas of the brain, such as the cerebellum, which don't appear to be massively affected in ALS and FTD. They are also not found in the same neurons as TDP-43 inclusions, which do coincide with areas of neurodegeneration (Balendra et al, 2018). In contrast to this, another explanation is that TDP-43 pathology is a downstream consequence of DPR toxicity. In a study by Ryan et al, (2022) Poly-GR, PR, and GA all caused structural damage to the nucleus and nuclear membrane, and the mislocalisation of Ran and RanGAP, resulting in defective NCT. The mislocalised TDP-43 co-occurred with the DPR-induced Ran and RanGAP mislocalisation, implying a potential link between the defective NCT driving the TDP-43 cytoplasmic inclusions. However, as none of these mechanisms can be definitively labelled as the cause of neurodegeneration, other targets may be worth investigating.

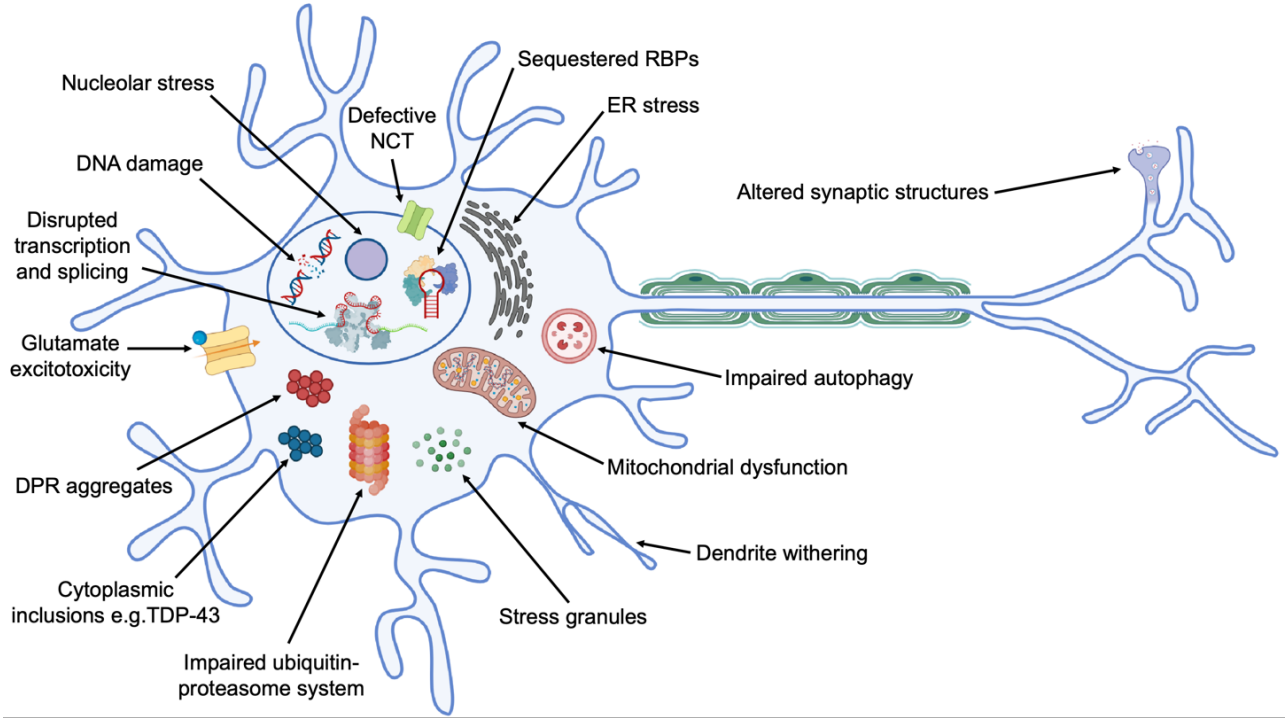

Figure 3: Impaired cellular processes in C9orf72 ALS-FTD
C9orf72 loss of function and toxic gain of function mechanisms have implications on a number of cellular processes. C9orf72 haploinsufficiency has been associated with impaired autophagy, increased glutamate receptors causing excitotoxicity, and inability to clear cytoplasmic inclusions and DPR aggregates. RNA foci toxicity causes secondary structures such as R-loops which sequester RBPs as well as aborted transcription, defective RNA processing and higher levels of nucleolar stress. DPRs have been shown to also induce nucleolar stress and disrupt RNA synthesis and splicing. As well as that they disrupt mitochondrial function, nucleocytoplasmic transport, affect the formation of stress granules, cause dendrite withering, alter synaptic structures which promotes glutamate release, and induces ER stress through defects in the ubiquitin-proteasome system. Created with BioRender.com

1.4. DNA damage in neurodegenerative disorders

A key feature of neurodegenerative diseases is the presence of DNA damage and defective DNA repair mechanisms. Increased levels of DNA damage have been seen in the brains of Alzheimer's disease (AD), Parkinson's disease (PD), Huntington's disease (HD), and ALS patients (Simpson et al, 2015; Milanese et al, 2018; Mitra et al, 2019; Thadathil et al, 2019).

1.4.1. DNA damage

DNA damage is a constantly occurring phenomenon; every cell is believed to accumulate 10^4- 10^5 DNA lesions every day (Giglia-Mari, Zotter, and Vermeulen, 2011). Damage can be caused by exogenous sources, such as ultraviolet and ionising radiation, chemical agents, and environmental agents, or endogenous sources, which include reactive oxygen species (ROS) generated from cellular metabolism, errors in replication, methylation, and deamination (Martin, 2008; Chatterjee and Walker, 2017).

The DNA damage caused occurs in a number of different forms. Bulky helix distorting lesions are often caused from UV radiation and ROS, whilst base mismatches from insertions or deletions are normally a result of replication error. Damage of a single nucleotide base from oxidation, deamination, depurination, or depyrimidination, or breakages in DNA strands, including both single strand breaks (SSBs) and double strand breaks (DSBs), can be a result of a number of damaging factors including ROS and X-rays. (Jeppesen, Bohr, and Stevnsner, 2011). Of all the forms of DNA damage, DSBs are the most toxic. If not repaired by the DNA damage response (DDR), DSBs will cause cell cycle arrest and apoptosis (Provasek et al, 2022).

1.4.2. The DNA damage response

DNA damage is able to initiate a cascade of repair mechanisms specific to the type of damage that has occurred. There are 5 major pathways: nucleotide excision repair (NER), mismatch repair (MMR), base excision repair (BER), homologous recombination (HR) and non-homologous end-joining (NHEJ) (Jeppesen, Bohr, and Stevnsner, 2011).

NER recognises the bulky, structurally distorting lesions. Whether they occur specifically on the transcribed DNA strand within active genes, or just throughout the genome dictates the type of NER; transcription-coupled NER (TC-NER), or global genome NER (GG-NER)

(Konopka and Atkin, 2022). GG-NER relies on XPC, a DNA binding protein which binds to the distorted structure in the damaged DNA, coupled with RAD23B for recognition of the damage site, followed by endonucleases to excise the damaged strand, and replication proteins to repair the gap. TC-NER is used when RNA polymerase II is stalled by a blockage on the transcribed strand. Cockayne syndrome protein A (CSA), a transcription factor of RNA polymerase I), and Cockayne syndrome protein B (CSB), a chromatin remodeller, initiate TC-NER and recruit transcription factor IIH (TFIIH) for the reverse translocation of RNA polymerase II. The lesion is then repaired in a similar fashion to GG-NER post-recognition (Jeppesen, Bohr, and Stevnsner, 2011; Chatterjee and Walker, 2017; Konopka and Atkin, 2022).

MMR repairs damage that forms insertion-deletion loops as a result of replication or recombination error. MutSα and MutAβ are the proteins responsible for recognising the lesions, followed by MutL complexes that localise to regulate the excision of the mismatch. DNA synthesis and ligation is then carried out by POL δ, RFC, HMGB1, and LIG1 (Konopka and Atkin, 2022).

BER acts on the DNA damage of single nucleotide bases where there isn't any significant distortion to the DNA helix. There are two pathways of BER, the short patch repair, for when there is only a single damaged nucleotide, and the long patch repair, for two or more damaged nucleotides (Chatterjee and Walker, 2017; Alhmoud et al, 2020). The damaged bases are detected by DNA glycosylases, which excise the nucleotide through cleavage of the N-glycosidic bond, creating an apurinic/apyrimidinic site. APE1 with POLβ or POL δ/ε cleaves the phosphodiester bond 5' to the abasic site and fills the nucleotide gap, ligated by LIG1 and either the LIG3/XRCC1 complex, or FEN1 in the long patch repair (Chatterjee and Walker, 2017; Alhmoud et al, 2020; Konopka and Atkin, 2022).

In addition to the base modified lesions, the DDR must also repair DNA strand breakages. SSB repair (SSBR) is via a specialised BER mechanism. Much like the BER pathway, there are variations to the repair of SSBs dependant on their formation. When SSBs are created by direct oxidative damage from ROS, the long patch sub-pathway is initiated. The SSB is detected by PARP1 which recruits APE1, and FEN1, both of which are endonucleases, as well as PNKP and APTX, which both modify the broken DNA ends to be compatible for ligation, and finally the processivity factor for DNA polymerase, PCNA. DNA polymerase β (POLβ) and DNA polymerase δ/ε (POL δ/ε) then fill the ssDNA gap, and the DNA is ligated by DNA ligase 1 (LIG1) (Jeppesen, Bohr, and Stevnsner, 2011; Madabhushi, Pan and Tsai, 2014; Chatterjee and Walker, 2017). The short patch SSBR sub-pathway occurs when SSBs are caused indirectly from the cleavage of the phosphodiester backbone during BER. These are recognised by APE1 and will undergo end-processing similarly to the long patch sub-pathway. POLβ and LIG3 are then responsible for the gap-filling and ligation. Finally, SSBs caused during aberrant TOP1 activity follow a variation of the long patch sub-pathway, where the end-processing uses TDP1 to remove the TOP1 (Chatterjee and Walker, 2017).

DSBs are the most significant form of DNA damage as they are the most lethal. Cells are estimated to have between 10 and 50 DSBs every day (Provasek et al, 2022). The DDR utilises two different pathways to tackle DSBs: HR and NHEJ. HR has much greater precision than NHEJ, it uses the sister chromatid in close proximity as the template for error-free repair, but that does mean it is restricted to the late S/G2 phase of the cell cycle. NHEJ promotes the direct ligation of the broken DNA ends without the need for a template so can occur throughout the cell cycle, however it is largely error prone (Jeppesen, Bohr, and Stevnsner, 2011).

1.4.3. DNA damage response: DSB signalling

A key regulatory kinase of the DDR is the ataxia telangiectasia mutated (ATM) kinase. ATM is a member of the phosphatidylinositol-3-kinase-like kinase family (PIKKs) along with the other DDR kinases ATR and DNA-PK (Jeppesen, Bohr, and Stevnsner, 2011). ATM is central to activating all aspects of the DDR including DNA repair, cell-cycle arrest/checkpoint activation, and apoptosis, all shown in figure 4 (Madabhushi, Pan, and Tsai, 2014). ATM is activated via autophosphorylation at Ser1981, following recruitment to the DSB site by the MRN complex. The MRN complex is made up of Mre11, Rad50 and NBS1 and is one of the initial sensors of DSBs. Mre11 is the core of the MRN complex as it contains the binding domains for Rad50 and NBS1, as well as DNA. Rad50 is an ATPase which aids in DNA end tethering and the formation of the MRN complex, and NBS1 controls the protein-protein and protein-DNA interactions of the complex such as recruiting ATM (Qiu and Huang, 2021). The MRN complex is crucial for fast localisation of ATM to the damage site, but also plays further roles in DSB repair due to its exonuclease and endonuclease properties, such as DSB resection for repair and ATR activation (Maréchal and Zou, 2013; Thadathil et al, 2019).

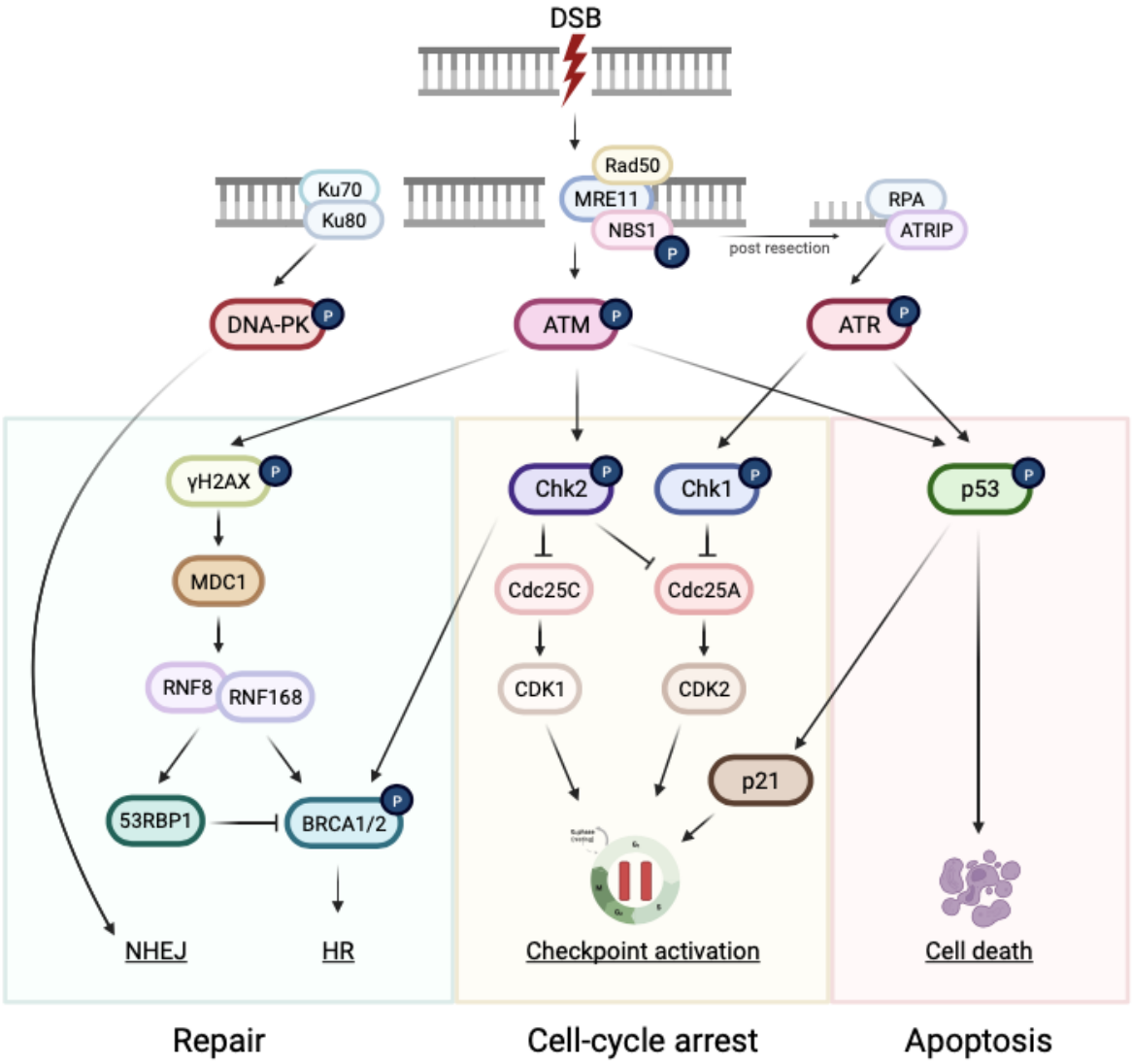

Figure 4: DDR signalling in response to DSBs
DSBs are identified by key sensors such as the MRN complex, Ku70/Ku80 and the RPA-ATRIP complex. The MRN complex binds to the break through MRE11, and NBS1 recruits ATM to the DSB site. This phosphorylates and activates ATM which in turn is able to initiate a number of signalling cascades. Phosphorylation of H2AX to γH2AX recruits MDC1, which in turn recruits RNF8 and RNF168. These form K63-linked ubiquitin chains which modify the chromatin to allow for further DDR protein recruitment. BRCA1 and 53BP1 localise to the break site and determine the repair pathway to be utilised. BRCA1 promotes HR, whilst 53BP1 facilities NHEJ, initiated from DSB sensing by Ku70/Ku80 and DNA-PK activation. ATM also activates Chk2, which inhibits Cdc25 proteins through phosphorylation. This prevents the dephosphorylation and activation of CDKs, arresting the cell cycle. A similar effect is seen by the ATR-Chk1 pathway, but ATR requires RPA-ssDNA bound by ATRIP for activation. The RPA-ssDNA is generated through DSB resection via the endo/exonuclease activity of the MRN complex. ATM and ATR can both activate p53 signalling, which can assist in checkpoint activation through p21 upregulation, or it can activate apoptotic pathways. Created with BioRender.com

Once activated, ATM can begin a number of signalling cascades to respond to the DSB. In both DSB repair pathways, ATM phosphorylates H2AX (γH2AX) forming nuclear foci, which have become a key marker for identifying the presence of DSBs (Konopka and Atkin, 2022). γH2AX amplifies the DDR signal by recruiting additional ATM, as well as attracting further DDR proteins (Reinhardt and Yaffe, 2009). MDC1 is one such protein which, following localisation to γH2AX, gets phosphorylated by ATM. MDC1 recruits RNF8 and RNF168 which form K63-linked ubiquitin chains causing chromatin modifications. This subsequently results in BRCA1 and 53RBP1 localisation, which both play a role in determining the appropriate repair pathway (Reinhardt and Yaffe, 2009; Shibata and Jeggo, 2021). BRCA1 promotes repair via HR, which can proceed following end-processing and resection at the break site. Rad51 binds to the ends forming a complex with BRCA1, BRCA2, Rad52 and Rad54 to find a homologous chromosome and create a displacement loop to use as a template. DNA polymerase uses the displacement loop to form the new DNA strand section which is ligated by LIG1 (Jeppesen, Bohr, and Stevnsner, 2011). 53BP1 indirectly promotes repair by NHEJ as an inhibitor of BRCA1 accumulation at DSB sites, rather than being a component of the pathway. In NHEJ, the DNA sensor is the Ku70/Ku80 heterodimer which recruits DNA-PK to the DSB. The end-processing factors tyrosyl-DNA-phosphodiesterase 1 (TDP1), flap structure-specific endonuclease 1 (FEN1), Werner syndrome helicase (WRN) and Artemis modify the DSB through DNA end resection so that DNA-PK recruits the LIG4-XRCC4-XLF complex for ligation (Jeppesen, Bohr, and Stevnsner, 2011; Gupta et al, 2014). As neurons are post-mitotic cells, the main repair pathway for DSBs in the brain is NHEJ (Konopka and Atkin, 2022).

In response to DSBs, ATM activates a signalling cascade to arrest the cell cycle, allowing time for the DNA repair pathways above to take place. It phosphorylates the checkpoint kinase Chk2, which has also been implicated in the mediation of DSB repair by

phosphorylating BRCA1 and BRCA2. Chk2 arrests the cell cycle at G1/S and G2/M by phosphorylating members of the cdc25 family. Phosphorylation of Cdc25A inhibits it from dephosphorylating and subsequently activating CDK2, without which cells are unable to progress from G1 to S phase. Similarly, phosphorylation of Cdc25C by Chk2 prevents the activation of CDK1, halting the G2/M phase transition (Zannini, Delia, and Buscemi, 2014). G1/S phase transition is also inhibited by the upregulated expression of p21, as a result of ATM phosphorylation of p53. When p53 is activated by ATM it promotes expression of proteins for checkpoint activation until the levels of DNA damage is irreparable, following which it drives the expression of proteins required for apoptosis such as PUMA and CD95 (Zannini, Delia, and Buscemi, 2014; Zhu et al, 2019).

1.4.4. DNA damage causes neurodegeneration in ALS-FTD

Mature neurons are traditionally believed to stay in the G0 phase of the cell cycle due to being post-mitotic. Increasing studies are now showing that in response to persistent DNA damage, neurons appear to re-enter the cell cycle at G1 (Fielder, Von Zglinicki, and Jurk, 2017; Shadfar, Brocardo, and Atkin, 2022). The formation of γH2AX in response to DNA strand breaks is slower in neurons than in proliferating cells, so initial signalling is more reliant on the ATM-Chk2 cascade to enforce the cell cycle arrest and DDR (Shadfar, Brocardo, and Atkin, 2022).

DNA damage is evident in ALS-FTD. Key markers of DSBs and apoptosis induction, γH2AX and p53, are shown to be upregulated in post-mortem brains and spinal cords of ALS patients. (Farg et al, 2017; Shadfar, Brocardo, and Atkin, 2022; Konopka and Atkin, 2022). The DSB accumulation in ALS patients has been shown to be coupled with TDP-43 cytoplasmic aggregates, a key pathogenic hallmark of ALS and FTD (Zhu et al, 2019). In

addition to its roles in RNA processing, such as transcription, splicing, and transport, TDP-43 is also a component of the DDR. It is recruited to the sites of DSBs along with Ku70 and the XRCC-4-LIG4 complex, facilitating repair via NHEJ (Zhu et al, 2019; Konopka and Atkin, 2022). Loss of TDP-43 due to its mislocalisation therefore hinders DSB repair causing accumulations of DSBs and chronic activation of the DDR (Fielder, Von Zglinicki, and Jurk, 2017; Thadathil et al, 2019).

Several mechanisms that are implicated in C9orf2 HRE pathogenicity also lead to DNA damage and genomic instability. This includes the secondary structures produced by the RNA foci, such as R-loops and G-quadruplexes, that have the potential to turn into SSBs and DSBs and activate the DDR, although they are also able to activate ATM even in the absence of DSBs suggesting that C9orf72 RNA foci directly contribute to the chronic activation of the DDR (Crossley, Bocek, and Cimprich, 2019). C9orf72 haploinsufficiency has been shown to impair autophagy causing the accumulation of protein aggregates such as TDP43 and p62. The accumulation of p62 impairs the DDR as p62 binds to and inhibits RNF168. This prevents the ubiquitination of H2AX and recruitment of repair proteins such as BRCA1, Rad51 and RAP80 (Wang et al, 2016). High levels of oxidative stress caused by mitochondrial dysfunction have been identified in C9orf72 neurons. This is known to be caused by the binding of DPRs, specifically poly-GR, to mitochondrial ribosomal proteins, resulting in the dysfunction (Lopez-Gonzalez et al, 2016). Oxidative stress is a key cause of DNA damage and Lopez-Gonzalez et al (2016) showed that suppression of oxidative stress significantly decreased the amount of poly-GR-induced damage in iPSC-derived C9orf72 motor neurons. All of these mechanisms, as well as many others, indicate that the DNA damage caused by C9orf72 pathogenicity, alongside impaired DDR, leads to unrepaired damage that persistently activates the DDR leading to neural dysfunction and apoptosis.

1.5. Project aims

Tuxworth et al (2019) have previously shown that inhibiting the DDR in a *Drosophila* Alzheimer's model was neuroprotective. A similar response has been seen in models of Huntington's disease where a reduction of ATM gene dosage improved neuropathology in a mouse model (Lu et al, 2014). This suggests that that the DDR might be a universal therapeutic target for neurodegenerative disease. This project aimed to characterise the *Drosophila* model of C9orf72 ALS-FTD by testing its motor defects and examining DSBs, and assess whether targeting the DDR would also prove to be neuroprotective in the *Drosophila* model of C9orf72 ALS-FTD.

2. Materials and Methods

2.1. *Drosophila* stocks and breeding

Drosophila stocks were bred on a standard media (50 g/L yeast, 50 g/L glucose, 0.8% agar, 1% soy flour) in vials kept at 18°C. For all experiments in adult *Drosophila*, expression of the neurodegeneration-associated transgenes was restricted to adult neurons by the use of the drug-inducible *elav;GAL4::GeneSwitch(GS)* driver line with a *white Dahomey (w^{DAH})* background. Expression was induced by addition of Mifepristone (ThermoFisher) to the standard media at a concentration of 200 µM. Virgin females of the driver line were crossed to males of the control and experimental lines. An example crossing scheme is shown below. The control line used was an isogenic w^{1118} strain. All *Drosophila* stocks were obtained from the Bloomington *Drosophila* stock centre, except for the DVglut-Gal4/QUAS-mCD8::6xGFP line used in the FlyClear protocol, which were a gift from Marko Pende (Medical University of Vienna).

Example Crossing Scheme:

Cross:

$$w^{DAH};\frac{+}{+};\frac{ElavGS}{ElavGS} \text{ virgin female flies} \quad \text{x} \quad w^{1118};\frac{UAS-G4C2}{cyo};\frac{tefu^{TRIP.GLOO138}}{Mkrs,Sb} \text{ male flies}$$

Progeny:

$$w;\frac{UAS-G4C2}{+};\frac{ElavGS}{tefu^{TRIP.GL00138}}$$

When selecting the progeny, only flies that did not have curly wings or shortened bristles on the thorax were selected to ensure the desired genotype.

2.2. Identifying double strand DNA breaks in *Drosophila* larvae

To identify the presence of DSBs, *OK371-gal4,UAS-CD8::GFP* larvae were irradiated at 0 and 0.5 Gy to act as controls. W^{1118} and UAS-G_4C_2 (BDSC_84727) lines were crossed with the *OK371-gal4,UAS-CD8::GFP* driver line to see if it was possible to observe DSBs in the CNS of the UAS-G_4C_2 larvae. Irradiated larvae were left for 60 minutes prior to dissection.

2.2.1 Dissection of Larval CNS

Larvae were dissected in phosphate buffered saline (PBS) and fixed for 30 minutes in 3.7% formaldehyde in PBS. After washing for 2 x 10 minutes, CNSs were permeabilized in PBS + 0.3% triton X-100 then blocked in 1% bovine serum albumin in PBS + 0.3% triton X-100 for 1 hour. They were then incubated in mouse anti-phosphorylated H2Av (Developmental Studies Hybridoma Bank clone UNC93-5.2.1, 1:2500) and Alexa-488 anti-GFP (ThermoFisher AB_221477, 1:2500) overnight at 4°C. CNSs were washed in PBS + 0.3% triton X-100 for 4 x 10 minutes at room temperature (RT) then incubated in Alexa-568 anti-mouse secondary antibody (ThermoFisher AB_2534072, 1:500) for 2 hours at 4°C in the dark. After washing for 3 x 10 minutes, CNSs were mounted on slides in Fluroshield with DAPI (Abcam). The larvae were imaged using water immersion objectives on the Zeiss LSM880 inverted confocal microscope (Carl Zeiss), and the z-stack was converted to a maximum intensity projection in ImageJ.

2.3. Survival Assays

Males only were used for the survival assay to prevent eggs being laid in the media requiring it to be changed more frequently. 10 flies were housed in each vial which were kept at 25°C.

All flies in each vial eclosed on the same day and were put into vials within 24 hours of eclosion. Vials were stored horizontally to prevent premature death from getting stuck in the media. Flies were transferred into new vials every 10 days. For the genotypes with the addition of mifepristone to the media to induce expression, mifepristone was added at day 7 post-eclosion. The number of living flies remaining in each vial was recorded each day until no living flies remained.

2.4. Movement Tracking with DART

20 flies were put into individual 65 x 5 mm locomotor tubes (Trikinetics) with standard media at one end covered by a rubber cap and cotton wool sealed the other end of the tube. Flies were transferred into new vials every 7 days. Males only were used for the movement tracking to prevent eggs being laid in the small amount of food requiring it to be changed more frequently. When not being recorded, tubes were kept at 25°C. Tubes were moved to the recording set-up 1 hour before the start of the recording to acclimatise to the RT and returned to 25°C after recording. Recordings were taken at around the same time each day.

Movement was recorded from above by a Logitech C920 HD camera at 5fps. The experimental paradigm was controlled by DART software running in MATLAB 2017a. It recorded for 5 minutes to establish a baseline movement speed, followed by 8 vibrational stimuli of 5 x 0.5 second bursts with 0.1 seconds between, at 10-minute intervals between stimulus events. The mean speeds of the 20 flies before stimulation and in response to stimulation are quantified by DART. 3 pre-induction days were recorded to get a baseline speed prior to induction. This pre-induction speed was given the performance index value of 1, in which all post-induction recordings were normalised to. Mifepristone was added to the standard media in the genotypes where expression was being induced after the pre-

induction recordings. This was considered day 0. This meant that expression was being induced 7 days post-eclosion. A full description of this method is published by Taylor and Tuxworth (2019).

2.5. Identifying double strand DNA breaks in *Drosophila* adult brains

All flies were kept at 25°C. Flies that were having expression induced were put onto mifepristone 7 days post eclosion.

2.5.1. Dissection of *Drosophila* adult brains

Adult fly brains were dissected in PBS and fixed for 30 minutes in 3.7% formaldehyde in PBS. After washing for 2 x 10 minutes in PBS, they were put into PBS + 0.3% triton X-100 for 15 minutes then blocked in 1% bovine serum albumin in PBS + 0.3% triton X-100 for 1 hour. Brains were then incubated in mouse anti-phosphorylated H2Av (Developmental Studies Hybridoma Bank UNC93-5.2.1, 1:1000) and rat anti-Elav (Developmental Studies Hybridoma Bank 7E8A10, 1:100) for 72 hours. Brains were washed in PBS for 5 x 10 minutes, and then incubated in Alexa-488 anti-mouse (Jackson ImmunoResearch AB_2338840, 1:500) and Alexa-594 anti-rat (Jackson ImmunoResearch AB_2340689, 1:500) for 48 hours at 4°C in the dark. After washing, brains were mounted on slides in Fluroshield with DAPI (Abcam) and imaged using the LSM880 inverted confocal microscope (Carl Zeiss).

2.6. Validation of *Drosophila* genetics by PCR analysis

To validate the genetic components of the *Drosophila* lines, genomic DNA (gDNA) needed to be extracted from the flies to carry out a polymerase chain reaction (PCR).

2.6.1. DNA extraction

2 *Drosophila* are crushed in the bottom of a 1.5ml Eppendorf containing 50µL (25µL per fly) of squishing buffer using a pipette tip. Squishing buffer is made up of the components listed in table 2.1. Proteinase K is added fresh each use and is not part of the stock solution.

Solution is then heated to 65°C in a heat block for 10 minutes before being transferred to a water path at 37°C for 1 hour. Proteinase K is inactivated by heating to 95°C in a heat block for 3 minutes. Finally, it is spun briefly in a centrifuge and the supernatant containing the gDNA is transferred to a new Eppendorf. This is stored in a freezer at -18°.

Table 2.1: Squishing buffer components

Squishing Buffer Components	**Concentration**
TrisHCL, PH 8	10mM
EDTA	1mM
NaCl	25mM
Proteinase K	200g/ml

2.6.2. PCR

The gDNA extracted from the experimental flies were used in a PCR to confirm the presence of the UAS-G_4C_2 insert, and the UAS-*tefu* RNAi. PCR master mix was made on ice using

the components listed in Table 2.2. Template DNA was added after the master mix had been aliquoted into individual PCR tubes. Primers used at a concentration of 0.5μM in the PCRs are detailed in table 2.3.

PCR was run in a thermal cycler using the conditions outlined in table 2.4 unless otherwise stated. The PCR products were then run on a 1% agarose gel using the Thermofisher 1Kb plus DNA ladder with Blue Juice (10787018).

Table 2.2: PCR master mix

Master mix components	**Volume (μL)**
10X DreamTaq Green Buffer	5
DreamTaq Green DNA Polymerase	0.2
dNTP Mix, 10mM each (ThermoFisher #R0191)	0.5
Forward Primer (FP)	0.5
Reverse Primer (RP)	0.5
Template DNA	1
H_2O	17.3

Table 2.3: Primers used in PCR reactions to validate *Drosophila* genetics

Primer Name	**Sequence 5' – 3'**
Control Tefu FP	CTAGTTCTCCATCGGCACTT
Control Tefu RP	CTTATCCAGATCCTCTCGGC
Valium 1 FP	CGGCTCTAGTTCTTTGCAA
Valium 1 RP	AGGTAGGCATCACACACGAT
Valium 20 FP	ACCAGCAACCAAGTAAATCAAC
Valium 20 RP	TAATCGTGTGTGATGCCTACC
Valium 22 FP	GGTGATAGAGCCTGA

Valium 22 RP	TAATCGTGTGTGATGCCTACC
UAS 4	CTGCAACTACTGAAATCTGCCA
UAS 5	TGTCACACCACAGAAGTAAGG

Table 2.4: Thermocycling conditions for PCR

Cycle Step	Temperature (°C)	Time	Cycle number
Initial denaturation	95	120 seconds	1
Denaturation	95	30 seconds	30
Annealing	55 unless stated otherwise	30 seconds	30
Extension	72	60 seconds	30
Final extension	72	5 minutes	1

2.7. FlyClear

To determine if it was possible to fluorescently visualise the degeneration of motor neurons in the *Drosophila* legs the FlyClear protocol published by Pende et al (2022) was attempted.

The flies were first fixed in 4% paraformaldehyde (pH.8.5) at 4°C for 90 minutes in an Eppendorf Thermomixer. After washing in PBS for 3 x 20 minutes at 4°C, FlyClear solution-1 was added to the flies as well as Alexa-633 phalloidin antibody (ThermoFisher A22284, 1:400), and this was kept at 37°C in a shaking incubator for 5 days. FlyClear solution-1 consists of 8 wt% THEED, 5 wt% Triton X-100 and 25 wt% Urea. After 5 days, the flies were washed in PBS for 24 hours at 25°C. The legs were then dissected with forceps and mounted on slides in VECTASHIELD (Vector Laboratories, H-1000-10) for imaging using the LSM880 inverted confocal microscope (Carl Zeiss).

3. Results

3.1. Visualisation of DSBs in *Drosophila* larvae

As it has already been established, DSBs are a key feature of many neurodegenerative diseases. This includes ALS-FTD (Walker et al, 2017). It was therefore important that I determine whether DSBs were induced in my *Drosophila* C9orf72 ALS model.

I first used larvae from my OK371-gal4,UAS-CD8::GFP driver line and irradiated them with 0 and 0.5Gy to produce DSBs. OK371-gal4 uses a gene trap of the vesicular glutamate transporter (VGlut), therefore expressing GAL4 in glutamatergic neurons, including the motor neurons and in some interneurons in the CNS. The OK371-gal4 drives UAS-CD8:GFP in this line, which labels the neuronal cell bodies with GFP (green fluorescent protein) and thus enables the glutamatergic neurons to be able to be visualised by confocal microscopy after fixation and antibody staining. I irradiated the larvae, allowed them to recover for 60 mins which equates to the peak of the DNA damage response, then dissected the CNS out of the larvae. The dissected larvae were fixed and stained for an increase in γH2Av, the *Drosophila* homolog of mammalian γH2AX. This is a histone modification that accumulates at the sites of DSBs and is used as a standard marker for the presence of DSBs.

Figure 5 shows that 0.5Gy irradiation was sufficient to produce widespread yH2AV staining in the CNS, indicating the presence of DSBs. The staining was absent in the non-irradiated controls. 0.5Gy is a relatively low dose – cultured cells are routinely treated with 2-8 Gy of irradiation for studies looking at the DNA damage response and may represent as few as 5 – 10 DSBs per cell My hypothesis based on these results is that if DSBs were present in my G_4C_2 *Drosophila* model, then they would be detectable using anti-γH2Av staining.

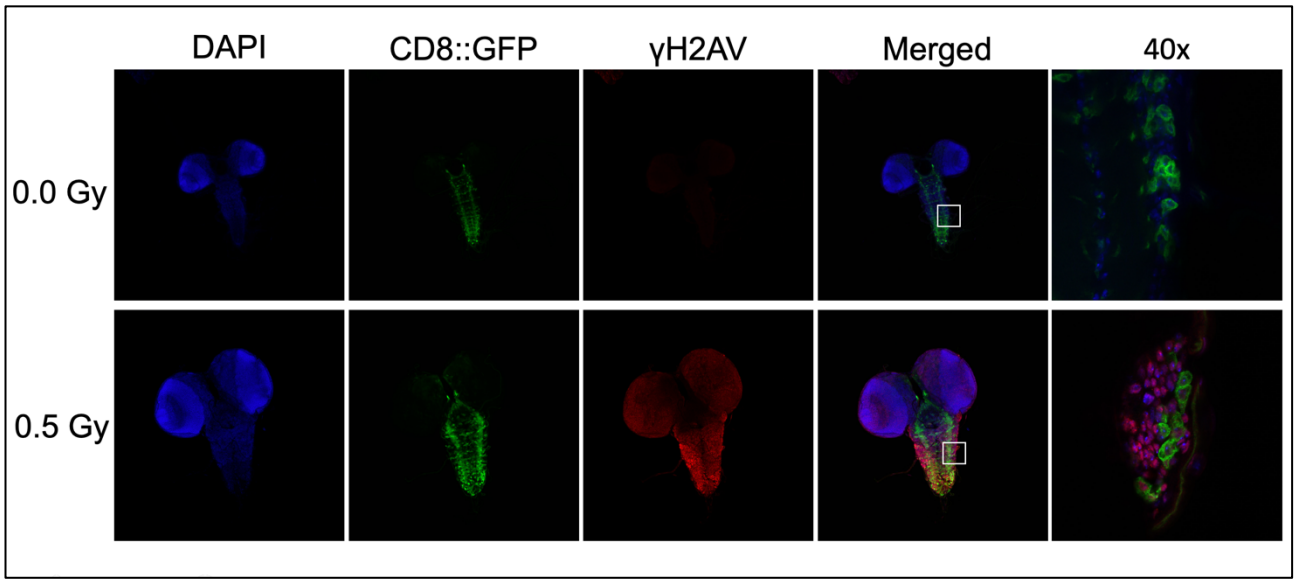

Figure 5: Irradiation with 0.5Gy produced a detectable level of DSBs in the larval CNS. *Cells were irradiated with 0.0 or 0.5Gy then fixed and stained for CD8::GFP (green, glutamatergic neurons), γH2Av (red, DSBs), and DAPI (blue, DNA). The larvae irradiated with 0.5Gy showed widespread DNA damage The larvae irradiated with 0.5Gy showed widespread DNA damage which was absent in the non-irradiated controls.*

3.1.1. DSBs are generated by expression of G_4C_2

The OK371-gal4,UAS-CD8::GFP driver was crossed to w^{1118} as a control, or to the UAS-G_4C_2 line, which contains 49 repeats of the GGGGCC HRE. I expected to see no detectable DBSs in the larvae from the w^{1118} cross, but that the DSBs would be detectable within the neuronal cell bodies the larvae from the UAS-G_4C_2 cross.

Figure 6 shows the images of larvae from the control w^{1118} and UAS-G_4C_2 crosses to OK371-gal4. Whilst both exhibited some background staining with anti-γH2Av, there was clearly stronger staining in the UAS-G_4C_2 crosses. Unexpectedly, while DSBs were present in the glutamatergic neurons that were marked with anti-GFP staining, there also appeared to be γH2Av+ staining in neighbouring, GFP negative cells, even though expression of G_4C_2 was restricted to the glutamatergic neurons by the OK371-gal4 driver. Another observation was that the UAS-G_4C_2 expressing larvae appeared to have lost the ordered, layered

structure of the optic neuropils (data not shown). This layered structure is seen in the control larvae and also in the irradiated larvae (see figure 5).

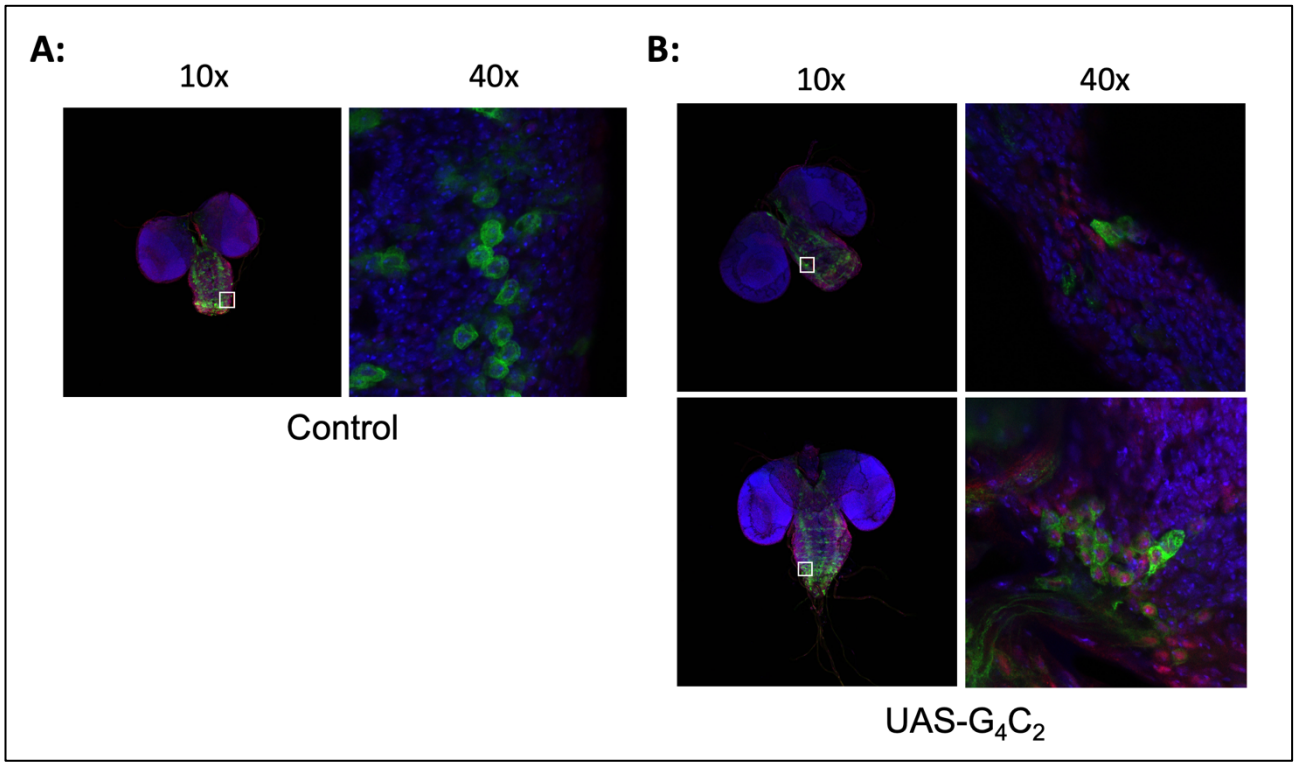

Figure 6: Widespread DNA damage detectable in UAS-G_4C_2 expressing larvae
OK371-gal4,UAS-CD8::GFP was crossed with the UAS-G_4C_2 line or w^{1118} as a control. Larval CNSs were dissected, fixed, and stained with anti-GFP (green, glutamatergic neurons), anti-γH2Av (red, DSBs), and DAPI (blue, DNA). (A) w^{1118} control larvae do not show any DSBs. The VNC does however appear to be slightly stunted. Background red signals not specific to yH2Av+ staining. (B) UAS-G_4C_2 larvae show yH2Av+ staining DSBs in the cell bodies of glutamatergic neurons (GFP+), as well as in the cell bodies of neighbouring GFP- cells.

3.2. Suppressing ATM expression improved lifespan in *Drosophila* C9orf72 model

DSBs accumulating in the CNS will chronically activate the DNA damage responses, including the critical ATM kinase. Having shown that DNA damage is accumulating in the CNS of G4C2-expressing flies, I now wanted to ask whether targeting the central ATM pathway would be neuroprotective in this model. I first used survival analysis to determine the effect on lifespan of the flies in which G4C2 expression was induced specifically in adult neurons and ask whether reducing ATM expression would promote increased survival.

ATM expression was reduced by expressing a UAS-shRNA line, UAS-tefu$^{TRIP.GL00138}$, which targets the *Drosophila* ATM orthologue, *telomeres fus*ed(*tefu*). shRNA expression is under UAS control in the Valium22 vector.

Both UAS-G_4C_2 and the *tefu* shRNA expression was driven under the control of the steroid inducible elav GeneSwitch (GS) gal4 driver. This allowed expression to be withheld during neural development to avoid potentially confounding effects of expressing neurotoxic, aggregating proteins during development. Expression using standard Elav-Gal4 would have begun during embryonic development and persisted throughout larval and pupal stages. Any effects, therefore, might be due to developmental abnormalities. Moreover, loss of ATM (and other components of the DDR) causes neurodevelopmental effects in human inherited conditions; use of ElavGS allowed these likely effects to be by-passed. Expression of G4C2 and *tefu* KD was induced by the addition of mifepristone to the standard media 7 days post the eclosion of the adult flies.

The control *w^{1118}* cross had a median lifespan of 43 days under our food and culture conditions. This contrasts with the flies expressing the UAS-G_4C_2 sequence, which had all died by day 20 of expression (Figure 7A; median lifespan = 14 days, $p<0.0001$ LogRank analysis). This shows that the *Drosophila* model of C9orf72 ALS is highly toxic in my hands and replicates significantly shortened lifespan seen in ALS patients. Expression of the tefu shRNA knockdown construct alone had very little effect on the median lifespan of the flies which is 44 days when compared to the control of 43 days. This did however show to be significantly different ($p =0.0215$, LogRank analysis) but this is most likely not to be of biological relevance. However, when paired with UAS-G_4C_2 expression, the tefu KD drastically improved the survival rate of the UAS-G_4C_2-expressing flies, with the flies

surviving to a similar lifespan as the controls (median lifespan = 46 days). This is a significant rescue compared to the flies only expressing the G_4C_2 sequence ($p<0.0001$, LogRank analysis) and shows that supressing ATM expression improved the lifespan in my *Drosophila* C9orf72 ALS model.

I also did a survival assay of a different *Drosophila* model of ALS which expressed the mutated superoxide dismutase 1 (SOD1) gene, the first gene to be implicated in ALS pathology and responsible for approximately 20% of familial cases (Rosen et al, 1993; Marangi and Traynor, 2015). However, this did not appear to have any neurotoxic effect to the lifespan of those flies when expression was restricted to adult neurons with ElavGS-gal4 (Figure 7B). This is in marked contrast to previous studies (Phillips et al, 1989) where SOD1 was expressed throughout development. It was, therefore, not possible to explore if the neuroprotective effect of the *tefu* KD is specific to the C9orf72 model of ALS, or if it can be seen across multiple ALS models.

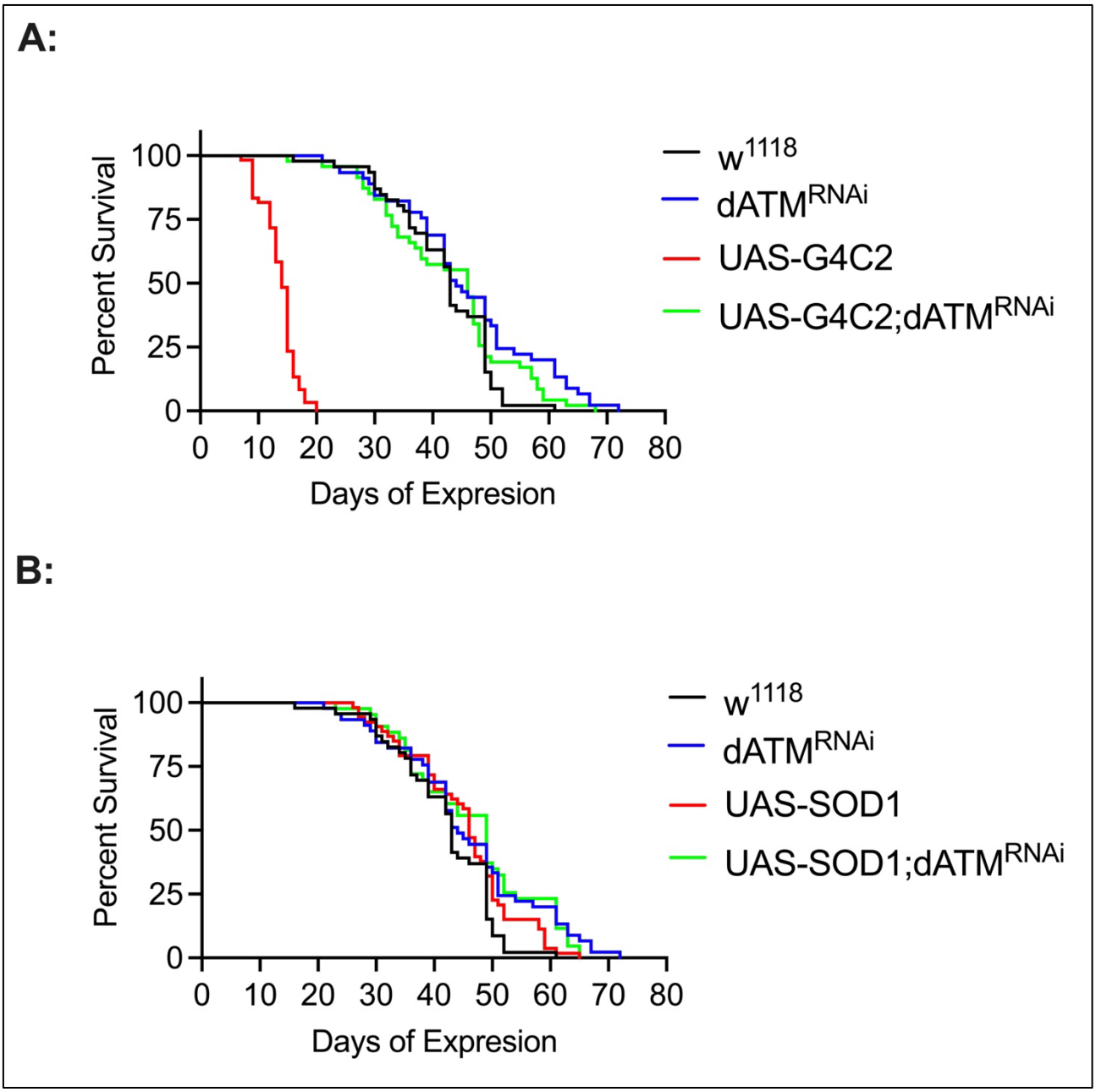

Figure 7: ATM knockdown improved the survival rate of the UAS-G_4C_2 model. *Graphs show the survival assays of two different Drosophila ALS models. The Log-rank (Mantel-Cox) test was used to compare groups.* ***(A) The survival rate of the UAS-G_4C_2 line with and without tefu KD, using w^{1118} as a control.*** *Significant reduction in the lifespan of the UAS-G_4C_2 expressing flies, with all flies having died by 20 days of expression (median lifespan = 14 days). Expression of Tefu KD ($dATM^{RNAi}$) alone had limited effect on the lifespan on the Drosophila compared to control w^{1118} cross, although this was statistically significant (p=0.0215, median lifespan of Tefu KD = 44 days, median lifespan of w^{1118} = 43 days). Combining expression of the UAS-G_4C_2 with the tefu KD result in a dramatic rescue of the toxicity caused by the expression of the G_4C_2 sequence (p<0.0001, median lifespan = 46 days).* ***(B) The survival assay of the mutated SOD1 line with and without tefu KD.*** *The mutant SOD1 expressing flies did not exhibit any toxicity, with no significant difference compared to the lifespan of the control (p=0.0848, median lifespan = 46 days).*

In accompaniment to the lifespan analysis where UAS-G_4C_2 and *tefu* RNAi expression was induced by mifepristone, the same genotypes were also assessed in the absence of mifepristone to evaluate the effectiveness of the GeneSwitch gal4 system. There have been previous reports of the GeneSwitch gal4 system being leaky, with low levels of expression present in the absence of mifepristone (Scialo et al, 2016). Figure 8 shows the lifespans of the genotypes with expression induced compared to those that weren't. Neurotoxicity was only seen in the UAS-G_4C_2 flies in the presence of mifepristone (median lifespan = 14 days), with all other genotypes displaying full lifespans (median lifespans range from 43-63 days). I am therefore confident that in the experimental models I am using, the GeneSwitch gal4 system is not leaky and will not have any detrimental impact on my experimental results.

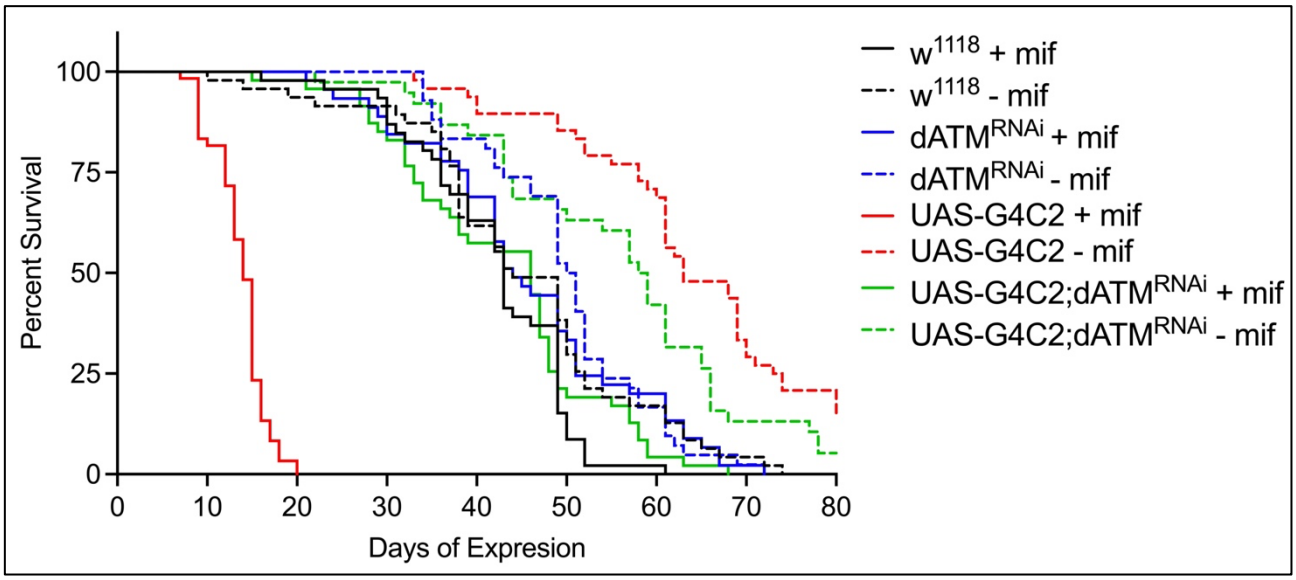

Figure 8: GeneSwitch gal4 system is not leaky in survival assay of UAS-G_4C_2
Graphs show the survival assay of the UAS-G_4C_2 and tefu KD lines both with and without induction of expression via addition of mifepristone to the fly food. As the UAS-G_4C_2 line only shows evidence of toxicity through a shortened lifespan when in the presence of mifepristone (median lifespan = 14 days, all other lifespans = 43-63 days), I can assume that the GeneSwitch gal4 system is not leaky.

3.3. Supressing expression of DDR proteins reduced motor deficits in the *Drosophila* C9orf72 model

One of the first visible features of ALS is muscle weakness and deterioration of motor control. This happens due to the progressive loss of motor neurons in the brain and spinal cord (Cleveland and Rothstein, 2001). After showing that targeting the central ATM pathway improved the lifespan of the flies expressing the G_4C_2 sequence, I now wanted to ask if reducing ATM expression would also improve motor function in G_4C_2 expressing *Drosophila*.

To test the effects of the G_4C_2 sequence and the *tefu* RNAi expression on *Drosophila* locomotor function, I used the DART software run in MATLAB 2017a, which has been previously adapted and used by the lab for targeting the DDR in an Aβ Alzheimer's model (Taylor and Tuxworth, 2019; Tuxworth et al, 2019). The DART system replaces the need for the traditional climbing assay where the percentage of adult flies that are able to climb up the side of the vial to a set distance is measured after the vial is tapped on a hard surface causing the flies to fall to the bottom (Gargano et al, 2005). The DART system instead applied 8 pulses of vibrational stimuli at 10-minute intervals to startle the flies which are housed individually in small vials. The movement of the flies up and down the vials increase in response to the stimulus, and this is tracked and quantified by the software. The DART assay is more consistent than the climbing assay and fewer flies are needed as a consequence.

I used the same expression system as the lifespan analysis, with both the UAS-G_4C_2 and the *tefu* shRNA expression being driven under the control of the steroid inducible elav GeneSwitch (GS) gal4 driver. Expression was induced by the addition of mifepristone to the standard media 7 days post the eclosion of the adult flies.

The *tefu* KD alone had very little effect on the motor function compared to the control (0.0209). Similar to the drastic decline seen in the lifespan, Figure 9 shows that the motor function of the G_4C_2 expressing flies is also significantly reduced compared to the control w^{1118} cross (p=0.0003, n=6, ANOVA). The flies expressing UAS-G_4C_2 and the *tefu* KD had a significantly slower rate of decline than the ones expressing G_4C_2 alone (p<0.0001, n=6, ANOVA) showing that reducing ATM expression is neuroprotective against the decline in motor function of G_4C_2 expressing *Drosophila*.

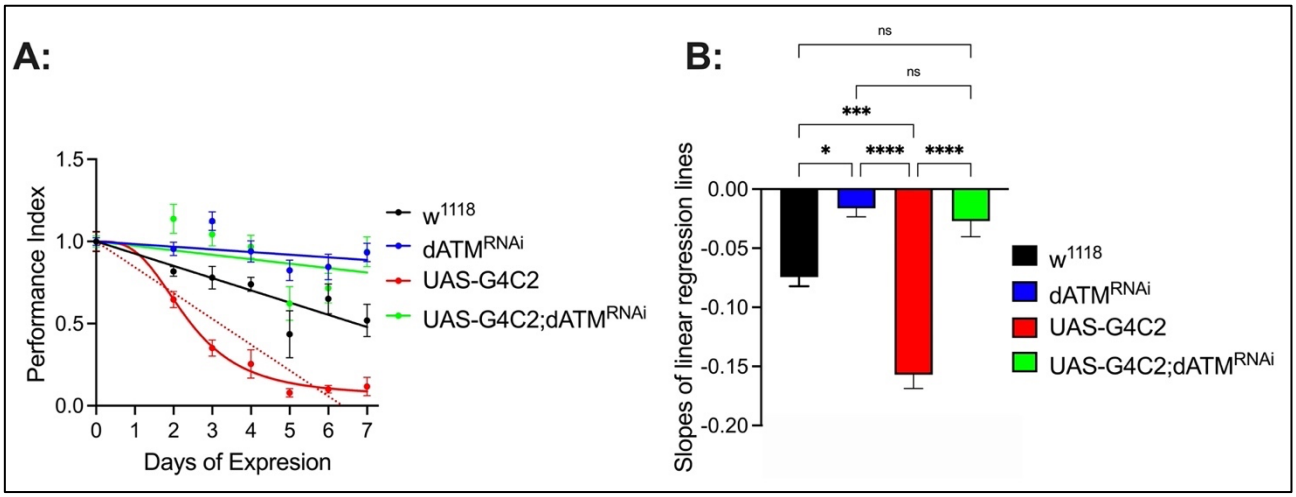

Figure 9: Knockdown of tefu expression rescued motor deficits of the G_4C_2 expressing Drosophila
(A) The performance index of the Drosophila models in response to vibrational stimuli. *Each data point is the mean amplitude with the S.E.M of the 20 (or however many left living) flies on each day that they are exposed to the stimuli. Linear regression lines were fitted, and the slopes were compared by ANOVA in B. The UAS-G_4C_2 expressing model response is better suited to a sigmoidal curve, also fitted.* ***(B) The rate of decline shown by the gradients of the linear regression lines.*** *The slope and S.E.M of the regression lines are plotted and were compared by an ordinary one-way ANOVA with Tukey's multiple comparisons test. The G_4C_2 expressing flies exhibited a greater rate of decline compared to the control (p=0.0003, =6). The tefu KD significantly rescues the rate of decline of the G_4C_2 expressing flies (p<0.0001, n=6).*

This result answered my original question of whether reducing ATM expression would also improve motor function in G_4C_2 expressing *Drosophila*, but I now wanted to confirm this finding by repeating the experiment using an independent shRNA to reduce *tefu* expression to ensure the results I was seeing were not due to a possible off-target effect of the shRNA.

I also wanted to ask whether I could elicit the same response by targeting the downstream target of ATM, Chk2, which previous work in the group had suggested was also a neuroprotective target (Taylor et al, 2022)

I repeated the experiment with the *tefu* shRNA (TRIP.GL00138) used in the experiment above but constructed into a new stock line with UAS-G_4C_2, as well as a different *tefu* RNAi (TRIP.JF01422), which is under UAS control in Valium 1 vector, and an RNAi line to knockdown Chk2 expression (TRIP.GL00020). Expression of the UAS-G_4C_2 and all knockdowns were again driven under the control of the steroid inducible elav GeneSwitch (GS) gal4 driver. Expression was induced by the addition of mifepristone to the standard media 7 days post the eclosion of the adult flies.

The UAS-G_4C_2 expressing flies still showed a significant increase in the rate of decline ($p=0.0352$), albeit a smaller increase than previously seen. However, this time expression of the G_4C_2 sequence with the *tefu* shRNA used previously (TRIP.GL00138) did not show any significant difference in the rate of decline compared to the UAS-G_4C_2 expressing flies ($p=0.3486$, figure 10A and B). This contradicts the previous experiment's finding that *tefu* knockdown improved motor function in G_4C_2 expressing *Drosophila*. The expression of the G_4C_2 sequence with a new *tefu* RNAi (TRIP.JF01422) also failed to show any significant difference in the motor function decline compared to the UAS-G_4C_2 expressing flies ($p>0.9999$, figure 10C and D). However, the Valium 1 vector which contained the TRIP.JF01422 RNAi has been identified as being weak in KD strength, which may explain why this RNAi line did not replicate the significant difference in the rate of decline compared to the UAS-G_4C_2 expressing flies that had been seen in the first experiment (Perkins et al., 2015).

The KD of Chk2 expression in the G_4C_2 expressing flies does not show any significant difference to the flies expressing G_4C_2 alone (p=0.7481, figure 10E and F), but as the KD of *tefu* did not elicit a response either, it makes it hard to comment on why the KD of Chk2 did not affect the motor function of the G_4C_2-expressing *Drosophila*.

Interestingly, both the *tefu* KD (TRIP.JF01422) and the Chk2 KD alone significantly improved the motor function decline of the flies compared to the control w^{1118} cross ($p<0.0001$ for both). This contradicts the previous experiment's findings that the *tefu* KD had very little effect on the lifespan and motor function of the flies compared to the control w^{1118} cross (see Figures 7 and 9).

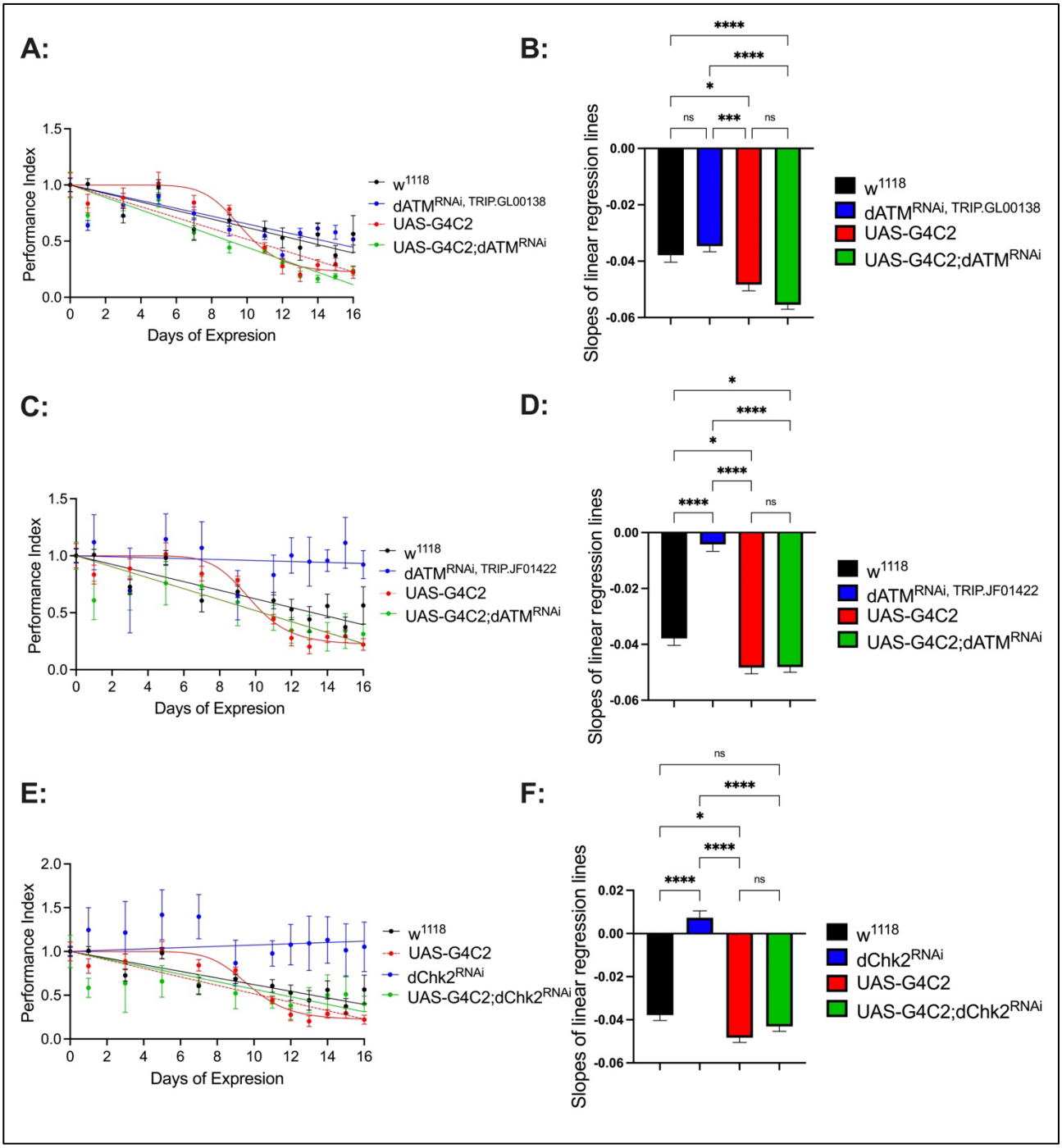

Figure 10: Knockdown of tefu and Chk2 expression did not confirm the previous experiment's results that reduced tefu expression improved the motor deficits of G_4C_2 expressing flies

A, C, and E show the performance index of the Drosophila models where each data point is the mean amplitude of the response and the S.E.M of the flies each day that they are exposed to the vibrational stimuli. Linear regression lines are fitted, and a sigmoidal curve is also shown on the graphs for the UAS-G_4C_2 expressing flies. B, D and F show the rate of decline by the slopes of the regression lines. The slope and S.E.M of the regression lines are plotted and were compared by an ordinary one-way ANOVA with Tukey's multiple comparisons test. The G_4C_2 expressing flies exhibited a slightly greater rate of decline compared to the control (p=0.0352). The tefu KD (TRIP.GL00138) in A and B was not significantly different to the rate of decline of the G_4C_2 expressing flies (p=0.3486, n=90). The tefu KD in C and D also did not show any significant difference to the G_4C_2 expressing flies (p=0.9999, n=90). KD of Chk2 in E and F did not have any effect on the rate of decline

of G_4C_2 expressing flies either (p=0.7481). Expression of Tefu KD (TRIP.JF01422) and Chk2 KD alone improved the rate of decline compared to the control w^{1118} cross (p<0.0001 for both, n=90).

3.4. RNAi lines used in the *Drosophila* C9orf72 model unable to be confirmed by PCR

Given the mixed results seen from testing the motor function of the G_4C_2 expressing flies with and without KD of the ATM pathway, I wanted to confirm that the shRNA expression I believed I was using when I produced the positive rescue result (see figure 9) was as expected. I did this by extracting gDNA from the stocks that I used for my experimental crosses and ran a PCR using primers recognising the pValium plasmid that the shRNA was inserted into.

The first *tefu* shRNA I used (TRIP.GL00138) was supposed to be under UAS control in pValium22. I ran a PCR on gDNA from my w^{1118} control stock, the TRIP.GL00138 line alone, the UAS-G_4C_2 line, and the stock containing both the UAS-G_4C_2 and TRIP.GL00138 used in the original experiment (Figure 10.2 A). I used the *tefu* primers as a control, and pValium22 primers to detect the presence of the *tefu* shRNA. All samples showed a band at around 300bp with the *tefu* primers showing the PCR had successfully amplified the samples. The Valium primers showed a band at around 350bp in the lane containing the gDNA of the TRIP.GL00138 alone stock confirming that the *tefu* shRNA was present in that line. There was no band present in the w^{1118}, UAS-G_4C_2, or UAS-G_4C_2;TRIP.GL00138 stocks. This implies that the *tefu* shRNA is not present in the UAS-G_4C_2;TRIP.GL00138 stock.

I ran a second PCR to test if the line that I believed to contain the TRIP.GL00138 *tefu* shRNA was actually under control of UAS in Valium1 instead of Valium22 (Figure 10.2 B). This would mean the stock would actually contain the TRIP.JF01422 *tefu* RNAi which is under

UAS control in Valium 1 and was used in my repeated motor function experiments (see figure 10). I again used the *tefu* primers as a control. The gDNA samples used in this PCR were from my w^{1118}, TRIP.JF01422, and UAS-G_4C_2;TRIP.GL00138 stocks. All 3 gDNA samples produced a band of around 300bp with the *tefu* control primers showing a successful PCR. A strong band was seen at around 200bp from the gDNA of the TRIP.JF01422 stock with the Valium1 primers. Very faint bands of the same size were seen in the w^{1118} and the UAS-G_4C_2;TRIP.GL00138 stocks. As it was highly likely these bands were a result of spill over from the lane containing the TRIP.JF01422 gDNA, the PCR was repeated. The same 3 bands were seen from the *tefu* control primers, but this time only a single band at around 200bp was seen in the TRIP.JF01422 lane with the Valium 1 primers. This suggests that it is not the TRIP.JF01422 *tefu* shRNA which is present in the UAS-G_4C_2;TRIP.GL00138 stock either.

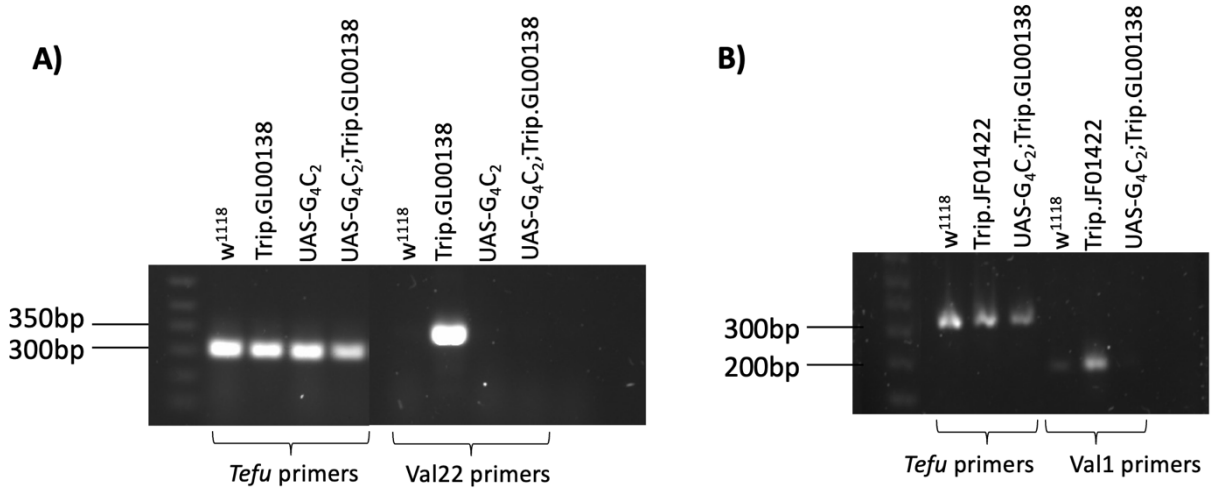

Figure 10.2: PCR data did not identify the RNAi experimental lines used.
A) shows the PCR data to detect the RNAi in the Valium 22 vector, with tefu primers used as a control. The RNAi was only detected in the TRIP.GL00138 alone stock and not the UAS-G_4C_2;TRIP.GL00138 stock. B) shows the PCR data to detect the RNAi in the Valium 1 vector, with tefu primers used as a control. The RNAi was only detected in the TRIP.JF01422 alone stock and not the UAS-G_4C_2;TRIP.GL00138 stock.

With both PCR results unable to confirm the identity of the 3rd chromosome insert I was unable to confirm if the UAS-G_4C_2;TRIP.GL00138 stock I used for the first motor function experiment (see figure 9) does contain the *tefu* shRNA.

Another way to confirm that KD of the ATM pathway had occurred would be to use qPCR. This would allow me to understand the efficiency of the RNAi KD, if there is any, by looking at the mRNA levels and therefore levels of gene expression. This would conclude whether a KD of the ATM pathway had occurred, but it would still not tell me which plasmid the shRNA had been inserted into in my experimental *Drosophila* line.

3.5. An increase in DSBs wasn't observed in *Drosophila* adult brains of the C9orf72 model

I previously showed that DSBs were accumulating in G_4C_2 expressing larvae. As ALS-FTD is an adult-onset disease, I wanted to repeat this experiment but withhold expression of the G_4C_2 during neural development and instead restricting expression to neurons in adult *Drosophila*. I therefore drove expression of the UAS-G_4C_2 under the control of the steroid inducible elavGS gal4 driver. Expression of G4C2 was induced by the addition of mifepristone to the standard media 7 days post the eclosion of the adult flies.

Anti-γH2Av detects a phosphorylated histone and in Drosophila cells, this appears in two clusters per cell which are likely to be the centrosome organising complex. Hence, the control brains would be expected to show γH2Av staining. However, previous work in the group had demonstrated a clear increased in γH2Av foci in neurons expressing a tandem amyloid construct (Tuxworth et al, 2019), suggesting that, were G4C2 expression to generate significant levels of DSBs in the brains of the flies, it would be detectable above

background. Figure 11 shows the images of adult brains from the control w^{1118} and UAS-G_4C_2 crosses to elavGS gal4. Both exhibited staining for elav and γH2Av as expected but there was no clear difference in intensity between the staining for the control and G4C2-expressing brains.

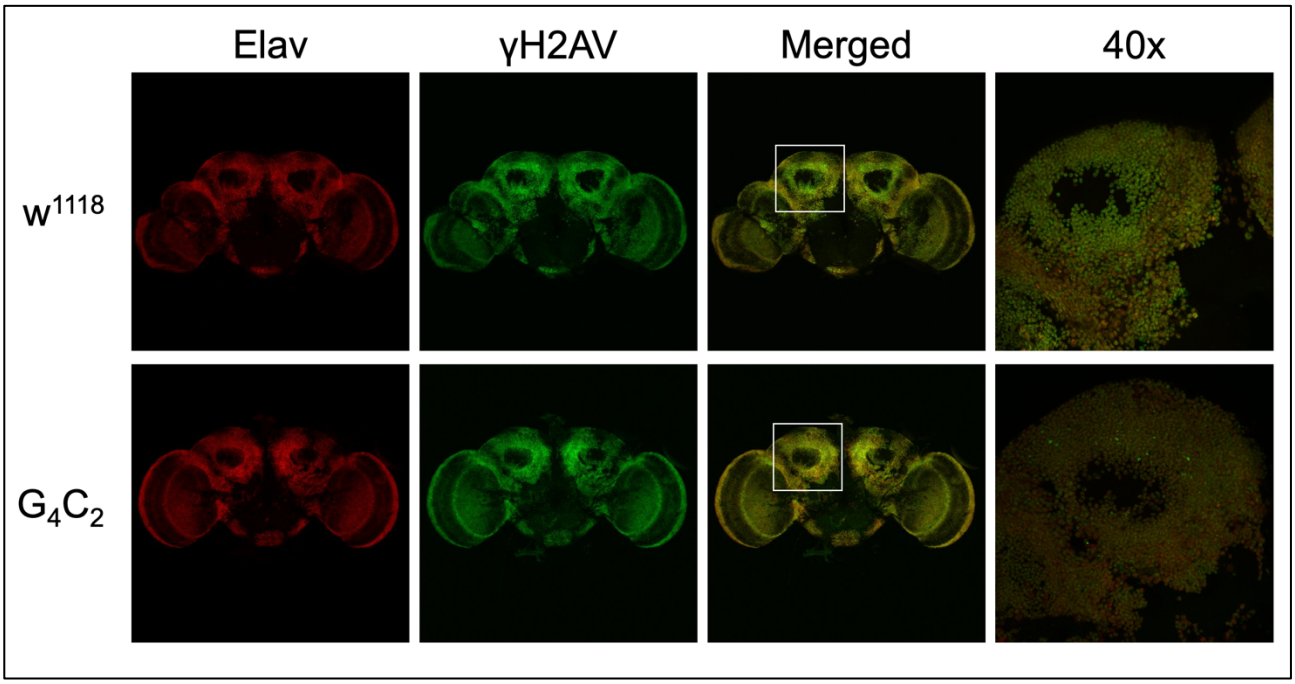

Figure 11: Staining for DSBs in adult Drosophila brains
elavGS was crossed with the UAS-G_4C_2 line or w^{1118} as a control. Expression was induced 7 days post the eclosion of the adult flies. Adult brains were dissected 16 days post induction, fixed, and stained with anti-elav (red, neurons), and anti-γH2Av (green, DSBs). Widespread elav+ and γH2AV+ staining is seen with no noticeable difference in both G_4C_2 expressing flies and the control w^{1118} cross.

3.6. Imaging the motor neurons of the *Drosophila* leg using the FlyClear protocol

The motor function loss in ALS-FTD is due to the degeneration of motor neurons in the brain and spinal cord which causes skeletal muscle denervation. I wanted to see if it would be possible to image this progressive denervation over time in my C9orf72 *Drosophila* model. A protocol has been developed which allows tissue-clearing and depigmentation of the *Drosophila* cuticle to be able to fluorescently visualise internal tissues and cells (Pende et al, 2022). I decided to use this protocol to see if it was possible to image the nerve innervation of skeletal muscle in *Drosophila* before using it with my experimental G_4C_2 line.

The *Drosophila* line used contained 6 copies of membrane GFP expressed in motor neurons to provide a bright motor neuron signal. After the fixing of the *Drosophila,* I included fluorescently labelled Phalloidin in the tissue-clearing solutions. Phalloidin stains actin filaments for visualisation of muscle fibres 1 (see methods).

The images produced are shown in Figure 12. The phalloidin staining does highlight skeletal muscle fibres, as expected and the membrane GFP has allowed for clear visualisation of the motor neurons. This protocol may need further adaptation, but it does show promising results that it will allow me to image the denervation that occurs in ALS in my *Drosophila* model.

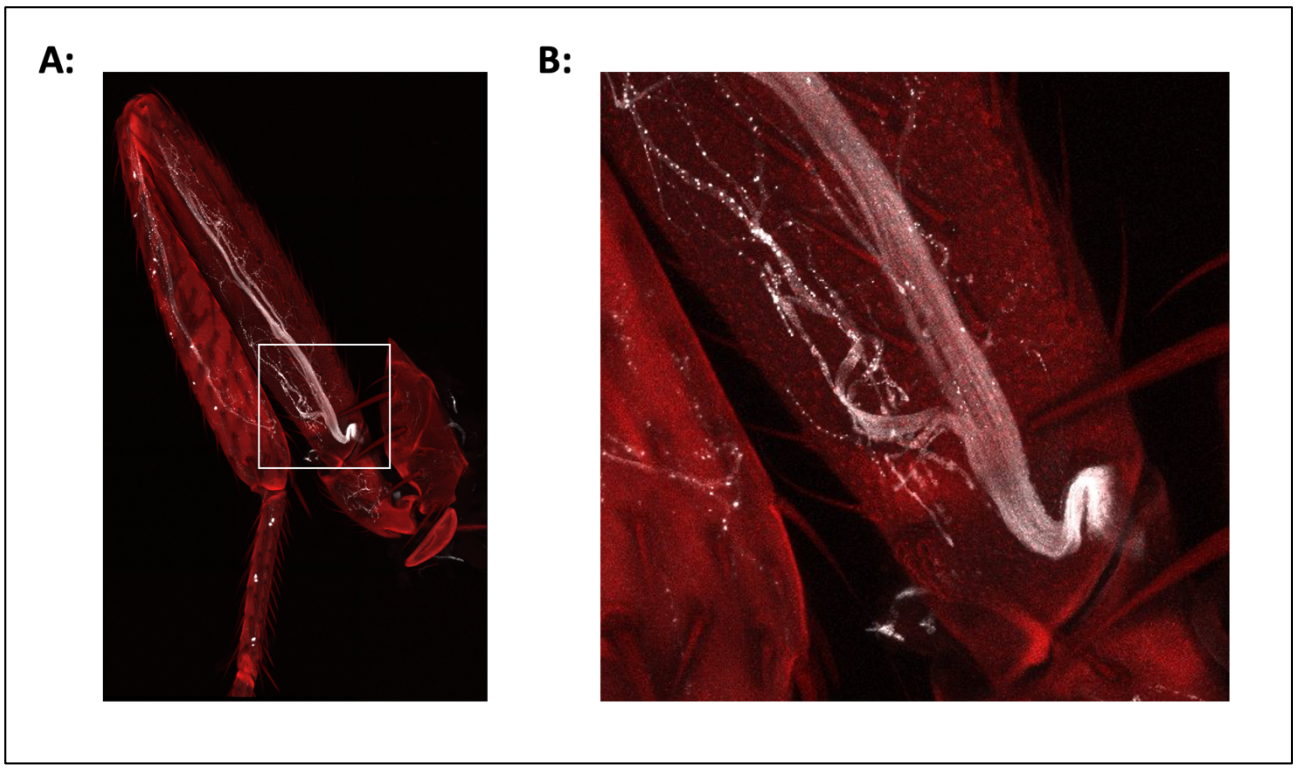

Figure 12: Imaging the skeletal muscle innervation of the Drosophila leg
Flies were fixed and then stained with Alexa-633 phalloidin and FlyClear solution 1 for depigmentation of the cuticle, prior to the dissection of the legs. The 6 copies of membrane GFP has given clear visualisation of the motor neurons. (A) shows 40x magnification of the Drosophila leg. (B) an enlarged image of the area indicated in A of the 40x magnification of the Drosophila leg.

4. Discussion

The aim of this project was to assess whether targeting the DDR would be neuroprotective in a *Drosophila* model of C9orf72 ALS-FTD. Double strand DNA breaks in DNA have been identified as a feature of a number of neurodegenerative diseases, such as Alzheimer's disease, Parkinson's disease, Huntington's disease, and amyotrophic lateral sclerosis (ALS) (Thadathil et al, 2019). Previous work in the group had already shown inhibiting the DDR to be neuroprotective in *Drosophila* Alzheimer's disease models (Tuxworth et al, 2019). This project showed DSBs to be a feature of the C9orf72 *Drosophila* model, and assessed the effect that DDR inhibition has on the lifespan and motor function of the flies.

4.1. DSBs were present in C9orf72 expressing *Drosophila* larval CNS but inconclusive in adult brains

DSBs have been shown to be a key feature of many neurodegenerative diseases, including ALS-FTD. They have been identified in post-mortem brains and spinal cords of ALS patients through the histone modification γH2AX, which accumulates at and around the site of the DSB and is used widely as a marker to quantify DSBs (Farg et al, 2017; Shadfar, Brocardo, and Atkin, 2022; Konopka and Atkin, 2022) For this reason, I looked for an increase in γH2Av, the *Drosophila* homolog of mammalian γH2AX, to identify DSBs in my experiments.

My results showed that DSBs were present in larvae expressing the dipeptide repeat sequence G_4C_2 that models the intronic expansion sequence seen in some cases of ALS-FTD. Anti-γH2Av+ positive staining was present in the cell bodies of glutamatergic neurons, marked with anti-GFP staining, but also in the cell bodies of neighbouring GFP- cells. Expression of the G_4C_2 sequence was restricted to glutamatergic neurons by the OK371-

gal4 driver, therefore DSBs were not expected to be present in GFP- negative cells. A reason for why damage could be present in cells outside of the glutamatergic neurons is the possibility of cell-to-cell transmission of DRPs. A study by Westergard et al, (2016) showed evidence of DPR transmission between neurons and a number of different glial cell types such as astrocytes, microglia, and oligodendrocytes. If this has occurred, then it is possible the DPRs are inducing DSBs in the neighbouring cells of the glutamatergic neurons providing an explanation for the additional damage seen (see figure 6). Identification of the neighbouring cells housing DSBs would help to understand if this is the case. Staining with the pan-glial marker, anti-repo would show if the neighbouring cells were glia; anti-elav would label all neurons. This might suggest that KD of DDR proteins such as ATM or Chk2 only in neurons would not be effective.

The larval CNSs from the control w^{1118} and UAS-G_4C_2 crosses to OK371-gal4 all appeared to have stunted ventral nerve cords (VNCs). This is not the case for the OK371-gal4 larvae that were irradiated. It is therefore possible that this is not biological damage that is being seen, but rather DNA damage resulting from the method of dissection. The CNSs were dissected by holding onto the cephalopharyngeal sclerites with one forcep, and the posterior end of the body with another forcep and pulling on the cephalopharyngeal sclerites to burst the cuticle and release the CNS and gut tissues. The CNS was then isolated from other structures. It was feasible that the pressure on the CNS from being pulled laterally was causing the changes in structures and damage that is seen (see figure 6). An alternative method of dissection is to use dissection scissors to cut the larvae body in the middle then, using forceps, roll the body wall inside out, revealing the CNS and gut tissues. This method reduces the physical pressure exerted on the CNS. Interestingly, the dissection method used for the irradiated larvae was the same as the method used for the w^{1118} and G_4C_2

crosses so it doesn't always cause structural damage, but this can be put down to human error.

Whilst DSBs were clearly identified in the CNS of G_4C_2 expressing larvae, this was not observed in the G_4C_2 expressing adult brains. There was no clear difference in the intensity of the anti-γH2Av staining between the control w^{1118} cross and the G_4C_2 expressing adult brains. This suggested that the G_4C_2 sequence had not generated significant levels of DSBs after 16 days of expression. The date of dissection was decided based on the results of the lifespan analysis, which determined the median lifespan of the G_4C_2 expressing *Drosophila* to be 14 days, with all flies having died by day 20 of expression. I therefore believed that by 16 days of expression a significant amount of DSBs would have been produced. Previous work by the group had shown an increase in γH2Av foci in neurons which expressed the tandem $A\beta_{1-42}$ oligomers in adult post-mitotic neurons. This had been seen following 30 days of expression, possibly suggesting that I had not been expressing my G_4C_2 HRE for long enough prior to dissection to generate a significant amount of DSBs, which is why I wasn't able to distinguish a difference between the intensity of anti-γH2Av staining. However, an alternative possibility is that expression of G_4C_2 in adult neurons either does not generate DSBs, or that they are present below the threshold of detection. γH2Av staining is detected in 1 or 2 spots per cell in a peri-nuclear location which is likely to be the centriolar organising centres. It is possible that a small amount of additional anti-γH2Av+ staining due to DSBs is not easily visible next to the centriolar organising centres, but in the case of the tandem $A\beta_{1-42}$ oligomers, many more DSBs were being generated.

4.2. ATM knockdown increased the lifespan of G_4C_2 expressing *Drosophila*

The life expectancy of patients with ALS is very short. This gets even shorter, 2 years from diagnosis compared to 3-5 years, in patients who also develop FTD (Ferrari et al, 2011). Expression of the G_4C_2 expansion in *Drosophila* mimics this diagnosis. My results showed a drastically shortened lifespan of G_4C_2 expressing flies (median lifespan = 14 days) compared to my control w^{1118} cross which had a median lifespan of 43 days. However, when *tefu* expression was reduced in the G_4C_2 expressing flies, the flies survived to a similar lifespan of the controls (median lifespan = 46 days). This shows that reducing ATM expression has a neuroprotective effect on the lifespan of the G_4C_2 expressing *Drosophila*.

Whilst the significant difference between the lifespan of the control w^{1118} cross and the G_4C_2 expressing flies is obvious, the difference between the other genotypes was less clear. Expression of the *tefu* shRNA knockdown construct alone appeared to have very little effect on the median lifespan of *Drosophila* compared to the controls (44 days and 43 days respectively). However, LogRank analysis of the data determined that there was a significant difference between these two data sets ($p = 0.0215$). The large number of flies I used in this experiment (100 flies per genotype) makes it likely that a very small change in the median lifespan could be identified as being statistically different. Whilst this is a small significant difference, it is not as large a statistical difference as is seen with the G_4C_2 expression compared to the controls ($p<0.0001$). Furthermore, the closeness of the median lifespans, 43 days and 44 days, leads me to conclude that whilst the expression of the *tefu* shRNA knockdown construct alone is significantly different to the control, it is not likely to be reflecting something of biological relevance.

The lifespan analysis also allowed me to conclude that my elavGS gal4 system I was using to drive expression in my experiments was not leaky. Previous studies had reported low levels of expression being present in the absence of mifepristone, which is used to induce

expression. This led them to determine that the GS system was leaky (Scialo et a, 2016). This is not a problem that I experienced. Neurotoxicity was only present in my G_4C_2 expressing flies which had been given mifepristone in the standard media to induce expression. All other genotypes, including the UAS-G_4C_2 x elavGS cross in the absence of mifepristone, displayed a full lifespan. Whilst I determined this to be sufficient proof that my elavGS driver was not leaky, there are other methods I could have utilised to evaluate this. A western blot can be used to show protein expression. However, in this case I believe that would be impractical. This is because dipeptide repeat protein have been shown to aggregate to form cytoplasmic inclusions (Ranganathan et al, 2020). These aggregates may prevent the DPRs from reliably entering an SDS-PAGE protein gel. To combat this I could have expressed a different protein via elavGS which I know would reliably enter an SDS-PAGE protein gel as a proxy for the DPR, to test if the elavGS system is leaky by western blot. Alternatively, using a fluorescent protein such as GFP as a proxy would allow me to look for expression with and without mifepristone using a fluorescent microscope.

The results were obvious that in the absence of mifepristone, expression was not induced, and all genotypes lived a full lifespan. However, there is a relatively large spread of the median lifespans of these genotypes (43 – 63 days). This is likely to be due to the genetic backgrounds of the genotypes being different. This has been shown to cause variability in phenotypes and survival (Evangelou et al, 2019). This variability can be reduced by backcrossing my stocks. For the purpose of this project, that would have been too time consuming and was not perceived to be necessary for the experiments I was doing, but it would be required in repeats to confirm the phenotypes seen.

As the C9orf72 mutation is only one of many mutations associated with ALS and FTD, I also performed the lifespan analysis expressing the mutated SOD1 gene. SOD1 is the second

largest contributor to ALS cases behind C9orf72 (Mejzini et al, 2019). Unfortunately, my model of SOD1 did not appear to exert toxicity as the lifespan of these flies had no significant difference to that of the controls. Multiple studies have previously shown otherwise, SOD1 mutations that render the protein inactive have displayed signs of shortened lifespans, motor deficits, and neurodegeneration (Phillips et al, 1989; Sahin et al, 2017). However, most studies used expression of SOD1 during developmental stages, whereas I restricted expression to adult neurons post-eclosion. Additionally, most studies used multiple copies of the UAS-SOD1 transgene – the line obtained from the Bloomington stock centre contains 4 copies – plus the drivers may well have been stronger. The lack of toxicity seen in my experiments may simply reflect a lower level of expression of SOD1. If that is the case, one has to consider how relevant a model of neurodegeneration is that requires huge levels of the SOD1 to be expressed in neurons. This meant it was not possible to explore if the neuroprotective effect of the *tefu* KD is specific to my C9orf72 model of ALS, or if it can also be neuroprotective in other *Drosophila* models of ALS. Accumulation of DNA damage as well as impaired DDR repair pathways are also implicated in SOD1 ALS cases as well as in C9orf72 ALS. This gave reason to believe that targeting the DDR would also be neuroprotective in SOD1 ALS given that we had seen a neuroprotective effect in C9orf72 ALS. If this had been seen, then it would support the idea that targeting the DDR might be neuroprotective in all cases of ALS. This would prevent limitations to therapeutic strategies which would only be suitable for C9orf72 cases of ALS.

4.3. The effect of ATM knockdown on motor deficits of G_4C_2 expressing *Drosophila*

Motor function deficits have been seen in previous studies modelling ALS in *Drosophila*, including models of the G_4C_2 expansion (Sahin et al, 2017; Sharpe et al, 2021). My model

of the G_4C_2 expansion also displayed a drastic decline in motor function in my hands. Much like the effect seen in the lifespan, reducing *tefu* expression in the G_4C_2 expressing flies was neuroprotective against the decline in motor function. The flies expressing both UAS-G_4C_2 and the *tefu* KD had a significantly slower rate of decline than the G_4C_2 expressing flies.

To analyse the differences between the genotypes, I fitted linear regression lines to each data set. However, it was clear that the rate of decline of the UAS-G_4C_2 expressing was better suited to a sigmoidal curve than a linear fit. This made statical analysis difficult as comparing the slopes of the linear lines, to the equation fitted to the sigmoidal curve is not possible using normal statistical methods. I consulted with biostatisticians about the best method of analysis of my data. We considered using simple comparisons between genotypes at a particular timepoint chosen from previous studies, but the day-to-day variability seen in all genotypes made that a poor choice. Plus, it would be cherry-picking a time point and ignoring the longitudinal trends. We also considered plotting area under the curve, but this ignores the fact that there is little difference between genotypes at early time points (as we would expect). The conclusion of the biostatisticians was that comparing linear slopes for all genotypes was the best method and would, if anything, reduce the differences between genotypes. Hence the strong statistical differences I identified were valid.

Unfortunately, PCR analysis was unable to confirm that the *tefu* shRNA knockdown construct was actually present in the flies which displayed this neuroprotective effect on motor function. On further inspection, I noticed that the *Drosophila* stock which contained the UAS-G_4C_2 on the second chromosome and *tefu* shRNA on the third, was being balanced on the third chromosome by MKRS, Sb. Balancer chromosomes are used to inhibit meiotic recombination and loss of mutations or transgenes. The MKRS, Sb balancer is a poor balancer as it does not inhibit recombination in quite large regions of the chromosome 3,

including the region containing the *tefu* shRNA construct. This would, therefore, have left the unbalanced sections open to potential translocation.

Upon reconstruction of the *tefu* shRNA into a new stock line with G_4C_2 I repeated the analysis of the motor function. This time, no neuroprotective effect was seen by the *tefu* KD, and the decline in motor function had no significant difference to the flies expressing G_4C_2 alone. This same result was seen with a different *tefu* shRNA as well as KD of Chk2 expression. These experiments did not replicate the results of the previous experiment I did, and alone would suggest that knockdown of the ATM-Chk2 pathway is not neuroprotective against the motor deficits seen in G_4C_2 expressing *Drosophila*. Whilst I knew that the shRNAs were present in the new constructed stock lines, I did not know how much they were actually reducing expression of *tefu* or Chk2 by when induced by mifepristone. One way to determine this would be to perform a qPCR. I began the process of doing this and established a protocol for extracting RNA and producing cDNA. Due to time constraints, I was unfortunately unable to run the qPCR of the cDNA samples I had produced. This would be important to do in the future to be able to conclude on the efficiency of the RNAi lines to be able to confidently determine what effect knockdown of the ATM-Chk2 pathway has on motor deficits seen in G_4C_2 expressing *Drosophila*. One other problem with these repeats of the experiments is that the G_4C_2-expression seemed to be much less toxic than in the first set of experiments. The only way to establish what's going on is to order the lines from the stock centre again, check all by sequencing and then rebuild all lines with sequencing after stock building again. Then, repeating the lifespans and motor analysis will give a definitive answer.

4.4. FlyClear protocol shows promise for imaging skeletal muscle denervation in G_4C_2 expressing *Drosophila*

The FlyClear protocol published by Pende et al, (2022) provided a novel opportunity for imaging internal structures of *Drosophila,* which removed most of the body and eye pigmentation without damaging morphology or quenching fluorescent signals. This presented the possibility of being able to image the skeletal muscle innervation in the *Drosophila* legs, and potentially measure the denervation which I believe is happening in my C9orf72 *Drosophila* model. The method described specified only the process of the tissue-clearing, with no mention of additional staining to the *Drosophila*. If I was going to be able to image the innervation of skeletal muscle, then I needed to have a marker for skeletal muscle as well as the 6 copies of membrane GFP expressed in motor neurons in the *Drosophila* line I was using. I included fluorescently labelled phalloidin into the clearing solution to stain actin filaments, which successfully highlighted skeletal muscle fibres in my images. This produced a clear visualisation of the motor neurons which innervate the skeletal muscle. Further adaptation is likely still necessary before using this protocol with the C9orf72 model. For example, I could include anti-DLG staining as a post synaptic marker or anti-Bruchpilot for staining of the presynaptic active zone. A timescale would also need to be decided for the when expressing the G_4C_2 sequence to ensure key events in the denervation process were not missed.

4.5. Therapeutic possibilities

Evidence to show that reducing expression of the DDR can be neuroprotective in Alzheimer's disease (Tuxworth et al, 2019), Huntington's disease (Lu et al, 2014) and now ALS, suggests that the DDR could be a universal target for neurodegenerative diseases.

Whilst ATM inhibition has shown to be neuroprotective in these models, it is unlikely to be a suitable target to use in therapy due to the number of downstream processes it regulates, having shown to have 700 phosphorylation targets as part of the DSB DDR (Lavin et al, 2015). It may therefore be beneficial to focus on other targets in the pathway as therapeutic interests, such as Chk2. Inhibition of Chk2 has been shown to also have a neuroprotective effect in a *Drosophila* Alzheimer's disease model, as well as in rat models of spinal cord injury (SCI) (Taylor et al, 2022). As Chk2 has a much lower number of phosphorylation targets, 24 proteins, then it is likely to have much less detrimental side effects for use in therapy. Future work may therefore be better suited to looking at the effects of Chk2 inhibition in more detail as this was only briefly touched upon in this project. Further analysis is also required into other models of ALS to ensure that these results are not C9orf72 dependant. Investigation into inhibiting the DDR in a TDP43 ALS model is currently being completed by the group.

5. References

Abramzon, Y.A., Fratta, P., Traynor, B.J. and Chia, R. (2020). The Overlapping Genetics of Amyotrophic Lateral Sclerosis and Frontotemporal Dementia. *Frontiers in Neuroscience*, 14. doi:https://doi.org/10.3389/fnins.2020.00042.

Alhmoud, J.F., Woolley, J.F., Al Moustafa, A.-E. and Malki, M.I. (2020). DNA Damage/Repair Management in Cancers. *Cancers*, [online] 12(4), p.1050. doi:https://doi.org/10.3390/cancers12041050.

Bahia, V.S., Takada, L.T. and Deramecourt, V. (2013). Neuropathology of frontotemporal lobar degeneration: a review. *Dementia & Neuropsychologia*, [online] 7(1), pp.19–26. doi:https://doi.org/10.1590/S1980-57642013DN70100004.

Balendra, R. and Isaacs, A.M. (2018). C9orf72-mediated ALS and FTD: multiple pathways to disease. *Nature Reviews Neurology*, 14(9), pp.544–558. doi:https://doi.org/10.1038/s41582-018-0047-2.

Burrell, J.R., Kiernan, M.C., Vucic, S. and Hodges, J.R. (2011). Motor Neuron dysfunction in frontotemporal dementia. *Brain*, 134(9), pp.2582–2594. doi:https://doi.org/10.1093/brain/awr195.

Callister, J.B. and Pickering-Brown, S.M. (2014). Pathogenesis/genetics of frontotemporal dementia and how it relates to ALS. *Experimental Neurology*, [online] 262, pp.84–90. doi:https://doi.org/10.1016/j.expneurol.2014.06.001.

Chatterjee, N. and Walker, G.C. (2017). Mechanisms of DNA damage, repair, and mutagenesis. *Environmental and molecular mutagenesis*, 58(5), pp.235–263. doi:https://doi.org/10.1002/em.22087.

Cleveland, D.W. and Rothstein, J.D. (2001). From charcot to lou gehrig: deciphering selective motor neuron death in als. *Nature Reviews Neuroscience*, 2(11), pp.806–819. doi:https://doi.org/10.1038/35097565.

Crossley, M.P., Bocek, M. and Cimprich, K.A. (2019). R-Loops as Cellular Regulators and Genomic Threats. *Molecular Cell*, 73(3), pp.398–411. doi:https://doi.org/10.1016/j.molcel.2019.01.024.

DeJesus-Hernandez, M., Mackenzie, Ian R., Boeve, Bradley F., Boxer, Adam L., Baker, M., Rutherford, Nicola J., Nicholson, Alexandra M., Finch, NiCole A., Flynn, H., Adamson, J., Kouri, N., Wojtas, A., Sengdy, P., Hsiung, Ging-Yuek R., Karydas, A., Seeley, William W., Josephs, Keith A., Coppola, G., Geschwind, Daniel H. and Wszolek, Zbigniew K. (2011). Expanded GGGGCC Hexanucleotide Repeat in Noncoding Region of C9ORF72 Causes Chromosome 9p-Linked FTD and ALS. *Neuron*, 72(2), pp.245–256. doi:https://doi.org/10.1016/j.neuron.2011.09.011.

Evangelou, A., Ignatiou, A., Antoniou, C., Kalanidou, S., Chatzimatthaiou, S., Shianiou, G., Ellina, S., Athanasiou, R., Panagi, M., Apidianakis, Y. and Pitsouli, C. (2019). Unpredictable Effects of the Genetic Background of Transgenic Lines in Physiological Quantitative Traits. *G3 Genes|Genomes|Genetics*, 9(11), pp.3877–3890. doi:https://doi.org/10.1534/g3.119.400715.

Farg, M.A., Konopka, A., Soo, K.Y., Ito, D. and Atkin, J.D. (2017). The DNA damage response (DDR) is induced by the C9orf72 repeat expansion in amyotrophic lateral sclerosis. *Human Molecular Genetics*, 26(15), pp.2882–2896. doi:https://doi.org/10.1093/hmg/ddx170.

Ferrari, R., Kapogiannis, D., D. Huey, E. and Momeni, P. (2011). FTD and ALS: A Tale of Two Diseases. *Current Alzheimer Research*, 8(3), pp.273–294. doi:https://doi.org/10.2174/156720511795563700.

Fielder, E., von Zglinicki, T. and Jurk, D. (2017). The DNA Damage Response in Neurons: Die by Apoptosis or Survive in a Senescence-Like State? *Journal of Alzheimer's Disease*, [online] 60(s1), pp.S107–S131. doi:https://doi.org/10.3233/JAD-161221.

Frick, P., Sellier, C., Mackenzie, I.R.A., Cheng, C.-Y., Tahraoui-Bories, J., Martinat, C., Pasterkamp, R.J., Prudlo, J., Edbauer, D., Oulad-Abdelghani, M., Feederle, R., Charlet-Berguerand, N. and Neumann, M. (2018). Novel antibodies reveal presynaptic localization of C9orf72 protein and reduced protein levels in C9orf72 mutation carriers. *Acta Neuropathologica Communications*, 6(1). doi:https://doi.org/10.1186/s40478-018-0579-0.

GARGANO, J., MARTIN, I., BHANDARI, P. and GROTEWIEL, M. (2005). Rapid iterative negative geotaxis (RING): a new method for assessing age-related locomotor decline in. *Experimental Gerontology*, 40(5), pp.386–395. doi:https://doi.org/10.1016/j.exger.2005.02.005.

Giglia-Mari, G., Zotter, A. and Vermeulen, W. (2010). DNA Damage Response. *Cold Spring Harbor Perspectives in Biology*, 3(1), pp.a000745–a000745. doi:https://doi.org/10.1101/cshperspect.a000745.

Goldman, J.S. and Van Deerlin, V.M. (2018). Alzheimer's Disease and Frontotemporal Dementia: The Current State of Genetics and Genetic Testing Since the Advent of Next-Generation Sequencing. *Molecular Diagnosis & Therapy*, 22(5), pp.505–513. doi:https://doi.org/10.1007/s40291-018-0347-7.

Gupta, A., Hunt, C.R., Chakraborty, S., Pandita, R.K., Yordy, J., Ramnarain, D.B., Horikoshi, N. and Pandita, T.K. (2014). Role of 53BP1 in the Regulation of DNA Double-Strand Break Repair Pathway Choice. *Radiation Research*, 181(1), pp.1–8. doi:https://doi.org/10.1667/rr13572.1.

Haeusler, A.R., Donnelly, C.J., Periz, G., Simko, E.A.J., Shaw, P.G., Kim, M.-S., Maragakis, N.J., Troncoso, J.C., Pandey, A., Sattler, R., Rothstein, J.D. and Wang, J. (2014). C9orf72 nucleotide repeat structures initiate molecular cascades of disease. *Nature*, [online] 507(7491), pp.195–200. doi:https://doi.org/10.1038/nature13124.

Hayashi, Y., Homma, K. and Ichijo, H. (2016). SOD1 in neurotoxicity and its controversial roles in SOD1 mutation-negative ALS. *Advances in Biological Regulation*, 60, pp.95–104. doi:https://doi.org/10.1016/j.jbior.2015.10.006.

HUDSON, A.J. (1981). AMYOTROPHIC LATERAL SCLEROSIS AND ITS ASSOCIATION WITH DEMENTIA, PARKINSONISM AND OTHER NEUROLOGICAL DISORDERS: A REVIEW. *Brain*, 104(2), pp.217–247. doi:https://doi.org/10.1093/brain/104.2.217.

Jeppesen, D.K., Bohr, V.A. and Stevnsner, T. (2011). DNA repair deficiency in neurodegeneration. *Progress in Neurobiology*, [online] 94(2), pp.166–200. doi:https://doi.org/10.1016/j.pneurobio.2011.04.013.

Jiang, J., Zhu, Q., Gendron, T.F., Saberi, S., McAlonis-Downes, M., Seelman, A., Stauffer, J.E., Jafar-nejad, P., Drenner, K., Schulte, D., Chun, S., Sun, S., Ling, S.-C., Myers, B., Engelhardt, J., Katz, M., Baughn, M., Platoshyn, O., Marsala, M. and Watt, A. (2016). Gain of Toxicity from ALS/FTD-Linked Repeat Expansions in C9ORF72 Is Alleviated by Antisense Oligonucleotides Targeting GGGGCC-Containing RNAs. *Neuron*, [online] 90(3), pp.535–550. doi:https://doi.org/10.1016/j.neuron.2016.04.006.

Johnson, B.S., Snead, D., Lee, J.J., McCaffery, J.M., Shorter, J. and Gitler, A.D. (2009). TDP-43 Is Intrinsically Aggregation-prone, and Amyotrophic Lateral Sclerosis-linked Mutations Accelerate Aggregation and Increase Toxicity. *Journal of Biological Chemistry*, 284(30), pp.20329–20339. doi:https://doi.org/10.1074/jbc.m109.010264.

Konopka, A. and Atkin, J.D. (2022). DNA Damage, Defective DNA Repair, and Neurodegeneration in Amyotrophic Lateral Sclerosis. *Frontiers in Aging Neuroscience*, 14. doi:https://doi.org/10.3389/fnagi.2022.786420.

Koppers, M., Blokhuis, A.M., Westeneng, H.-J., Terpstra, M.L., Zundel, C.A.C., Vieira de Sá, R., Schellevis, R.D., Waite, A.J., Blake, D.J., Veldink, J.H., van den Berg, L.H. and Pasterkamp, R.J. (2015). C9orf72 ablation in mice does not cause motor neuron degeneration or motor deficits. *Annals of Neurology*, 78(3), pp.426–438. doi:https://doi.org/10.1002/ana.24453.

Kwon, I., Xiang, S., Kato, M., Wu, L., Theodoropoulos, P., Wang, T., Kim, J., Yun, J., Xie, Y. and McKnight, S.L. (2014). Poly-dipeptides encoded by the C9orf72 repeats bind nucleoli, impede RNA biogenesis, and kill cells. *Science*, 345(6201), pp.1139–1145. doi:https://doi.org/10.1126/science.1254917.

Lavin, M., Kozlov, S., Gatei, M. and Kijas, A. (2015). ATM-Dependent Phosphorylation of All Three Members of the MRN Complex: From Sensor to Adaptor. *Biomolecules*, 5(4), pp.2877–2902. doi:https://doi.org/10.3390/biom5042877.

Lopez-Gonzalez, R., Lu, Y., Gendron, Tania F., Karydas, A., Tran, H., Yang, D., Petrucelli, L., Miller, Bruce L., Almeida, S. and Gao, F.-B. (2016). Poly(GR) in C9ORF72 -Related ALS/FTD Compromises Mitochondrial Function and Increases Oxidative Stress and DNA Damage in iPSC-Derived Motor Neurons. *Neuron*, 92(2), pp.383–391. doi:https://doi.org/10.1016/j.neuron.2016.09.015.

Lu, X.-H., Mattis, V.B., Wang, N., Al-Ramahi, I., van den Berg, N., Fratantoni, S.A., Waldvogel, H., Greiner, E., Osmand, A., Elzein, K., Xiao, J., Dijkstra, S., de Pril, R., Vinters, H.V., Faull, R., Signer, E., Kwak, S., Marugan, J.J., Botas, J. and Fischer, D.F. (2014). Targeting ATM ameliorates mutant Huntingtin toxicity in cell and animal models of Huntington's disease. *Science Translational Medicine*, 6(268). doi:https://doi.org/10.1126/scitranslmed.3010523.

Mackenzie, I.R., Rademakers, R. and Neumann, M. (2010). TDP-43 and FUS in amyotrophic lateral sclerosis and frontotemporal dementia. *The Lancet Neurology*, 9(10), pp.995–1007. doi:https://doi.org/10.1016/s1474-4422(10)70195-2.

Madabhushi, R., Pan, L. and Tsai, L.-H. (2014). DNA Damage and Its Links to Neurodegeneration. *Neuron*, [online] 83(2), pp.266–282. doi:https://doi.org/10.1016/j.neuron.2014.06.034.

Marangi, G. and Traynor, B.J. (2015). Genetic causes of amyotrophic lateral sclerosis: New genetic analysis methodologies entailing new opportunities and challenges. *Brain Research*, 1607, pp.75–93. doi:https://doi.org/10.1016/j.brainres.2014.10.009.

Marechal, A. and Zou, L. (2013). DNA Damage Sensing by the ATM and ATR Kinases. *Cold Spring Harbor Perspectives in Biology*, [online] 5(9), pp.a012716–a012716. doi:https://doi.org/10.1101/cshperspect.a012716.

Mariely DeJesus-Hernandez, Finch, C.A., Wang, X.Z., Gendron, T.F., Bieniek, K.F., Heckman, M.G., Aliaksei Vasilevich, Murray, M.E., Rousseau, L., Weesner, R., Lucido, A., Parsons, M., Chew, J., Josephs, K.A., Parisi, J.E., Knopman, D.S., Petersen, R.C., Boeve, B.F., Graff-Radford, N.R. and Jan de Boer (2017). In-depth clinico-pathological examination of RNA foci in a large cohort of C9ORF72 expansion carriers. *Acta Neuropathologica*, 134(2), pp.255–269. doi:https://doi.org/10.1007/s00401-017-1725-7.

Martin, L.J. (2008). DNA Damage and RepairRelevance to Mechanisms of Neurodegeneration. *Journal of Neuropathology & Experimental Neurology*, [online] 67(5), pp.377–387. doi:https://doi.org/10.1097/NEN.0b013e31816ff780.

May, S., Hornburg, D., Schludi, M.H., Arzberger, T., Rentzsch, K., Schwenk, B.M., Grässer, F.A., Mori, K., Kremmer, E., Banzhaf-Strathmann, J., Mann, M., Meissner, F. and Edbauer, D. (2014). C9orf72 FTLD/ALS-associated Gly-Ala dipeptide repeat proteins cause neuronal toxicity and Unc119 sequestration. *Acta Neuropathologica*, 128(4), pp.485–503. doi:https://doi.org/10.1007/s00401-014-1329-4.

Mejzini, R., Flynn, L.L., Pitout, I.L., Fletcher, S., Wilton, S.D. and Akkari, P.A. (2019). ALS Genetics, Mechanisms, and Therapeutics: Where Are We Now? *Frontiers in Neuroscience*, 13. doi:https://doi.org/10.3389/fnins.2019.01310.

Milanese, C., Cerri, S., Ayşe Ulusoy, Gornati, S.V., Plat, A., Gabriels, S., Fabio Blandini, Monte, Hoeijmakers, J. and Mastroberardino, P.G. (2018). Activation of the DNA damage response in vivo in synucleinopathy models of Parkinson's disease. *Cell Death and Disease*, [online] 9(8). doi:https://doi.org/10.1038/s41419-018-0848-7.

Mitra, J., Guerrero, E.N., Hegde, P.M., Liachko, N.F., Wang, H., Vasquez, V., Gao, J., Pandey, A., Taylor, J.P., Kraemer, B.C., Wu, P., Boldogh, I., Garruto, R.M., Mitra, S., Rao, K.S. and Hegde, M.L. (2019). Motor neuron disease-associated loss of nuclear TDP-43 is linked to DNA double-strand break repair defects. *Proceedings of the National Academy of Sciences*, 116(10), pp.4696–4705. doi:https://doi.org/10.1073/pnas.1818415116.

Mizielinska, S., Gronke, S., Niccoli, T., Ridler, C.E., Clayton, E.L., Devoy, A., Moens, T., Norona, F.E., Woollacott, I.O.C., Pietrzyk, J., Cleverley, K., Nicoll, A.J., Pickering-Brown, S., Dols, J., Cabecinha, M., Hendrich, O., Fratta, P., Fisher, E.M.C., Partridge, L. and Isaacs, A.M. (2014). C9orf72 repeat expansions cause neurodegeneration in Drosophila through arginine-rich proteins. *Science*, 345(6201), pp.1192–1194. doi:https://doi.org/10.1126/science.1256800.

Mizielinska, S., Lashley, T., Norona, F.E., Clayton, E.L., Ridler, C.E., Fratta, P. and Isaacs, A.M. (2013). C9orf72 frontotemporal lobar degeneration is characterised by frequent neuronal sense and antisense RNA foci. *Acta Neuropathologica*, 126(6), pp.845–857. doi:https://doi.org/10.1007/s00401-013-1200-z.

Moens, T.G., Partridge, L. and Isaacs, A.M. (2017). Genetic models of C9orf72 : what is toxic? *Current Opinion in Genetics & Development*, 44, pp.92–101. doi:https://doi.org/10.1016/j.gde.2017.01.006.

Nidheesh Thadathil, Hori, R., Xiao, J. and Mohammad Moshahid Khan (2019). DNA double-strand breaks: a potential therapeutic target for neurodegenerative diseases. *Chromosome Research*, [online] 27(4), pp.345–364. doi:https://doi.org/10.1007/s10577-019-09617-x.

Pende, M., Saghafi, S., Becker, K., Hummel, T. and Dodt, H. (2022). FlyClear: A Tissue-Clearing Technique for High-Resolution Microscopy of Drosophila. *Springer eBooks*, pp.349–359. doi:https://doi.org/10.1007/978-1-0716-2541-5_18.

Perkins, L.A., Holderbaum, L., Tao, R., Hu, Y., Sopko, R., McCall, K., Yang-Zhou, D., Flockhart, I., Binari, R., Shim, H.-S., Miller, A., Housden, A., Foos, M., Randkelv, S., Kelley, C., Namgyal, P., Villalta, C., Liu, L.-P., Jiang, X. and Huan-Huan, Q. (2015). The Transgenic RNAi Project at Harvard Medical School: Resources and Validation. *Genetics*, [online] 201(3), pp.843–852. doi:https://doi.org/10.1534/genetics.115.180208.

Phillips, J.P., Campbell, S.D., Michaud, D., Charbonneau, M. and Hilliker, A.J. (1989). Null mutation of copper/zinc superoxide dismutase in Drosophila confers hypersensitivity to paraquat and reduced longevity. *Proceedings of the National Academy of Sciences of the United States of America*, 86(8), pp.2761–2765. doi:https://doi.org/10.1073/pnas.86.8.2761.

Provasek, V.E., Mitra, J., Malojirao, V.H. and Hegde, M.L. (2022). DNA Double-Strand Breaks as Pathogenic Lesions in Neurological Disorders. *International Journal of Molecular Sciences*, [online] 23(9), p.4653. doi:https://doi.org/10.3390/ijms23094653.

QIU, S. and HUANG, J. (2021). MRN complex is an essential effector of DNA damage repair. *Journal of Zhejiang University. Science. B*, [online] 22(1), pp.31–37. doi:https://doi.org/10.1631/jzus.B2000289.

Ranganathan, R., Haque, S., Coley, K., Shepheard, S., Cooper-Knock, J. and Kirby, J. (2020). Multifaceted Genes in Amyotrophic Lateral Sclerosis-Frontotemporal Dementia. *Frontiers in Neuroscience*, 14. doi:https://doi.org/10.3389/fnins.2020.00684.

Reinhardt, H.C. and Yaffe, M.B. (2009). Kinases that control the cell cycle in response to DNA damage: Chk1, Chk2, and MK2. *Current Opinion in Cell Biology*, [online] 21(2), pp.245–255. doi:https://doi.org/10.1016/j.ceb.2009.01.018.

Renton, Alan E., Majounie, E., Waite, A., Simón-Sánchez, J., Rollinson, S., Gibbs, J. Raphael, Schymick, Jennifer C., Laaksovirta, H., van Swieten, John C., Myllykangas, L., Kalimo, H., Paetau, A., Abramzon, Y., Remes, Anne M., Kaganovich, A., Scholz, Sonja W., Duckworth, J., Ding, J., Harmer, Daniel W. and Hernandez, Dena G. (2011). A Hexanucleotide Repeat Expansion in C9ORF72 Is the Cause of Chromosome 9p21-Linked ALS-FTD. *Neuron*, 72(2), pp.257–268. doi:https://doi.org/10.1016/j.neuron.2011.09.010.

Robberecht, W. and Philips, T. (2013). The changing scene of amyotrophic lateral sclerosis. *Nature Reviews Neuroscience*, 14(4), pp.248–264. doi:https://doi.org/10.1038/nrn3430.

Rosen, D.R., Siddique, T., Patterson, D., Figlewicz, D.A., Sapp, P., Hentati, A., Donaldson, D., Goto, J., O'Regan, J.P. and Deng, H.X. (1993). Mutations in Cu/Zn superoxide dismutase gene are associated with familial amyotrophic lateral sclerosis. *Nature*, [online] 362(6415), pp.59–62. doi:https://doi.org/10.1038/362059a0.

Ryan, S., Rollinson, S., Hobbs, E. and Pickering-Brown, S. (2022). C9orf72 dipeptides disrupt the nucleocytoplasmic transport machinery and cause TDP-43 mislocalisation to the cytoplasm. *Scientific Reports*, [online] 12(1), p.4799. doi:https://doi.org/10.1038/s41598-022-08724-w.

Şahin, A., Held, A., Bredvik, K., Major, P., Achilli, T.-M., Kerson, A.G., Wharton, K., Stilwell, G. and Reenan, R. (2016). Human SOD1 ALS Mutations in a Drosophila Knock-In Model Cause Severe Phenotypes and Reveal Dosage-Sensitive Gain- and Loss-of-Function Components. *Genetics*, 205(2), pp.707–723. doi:https://doi.org/10.1534/genetics.116.190850.

Scialo, F., Sriram, A., Stefanatos, R. and Sanz, A. (2016). Practical Recommendations for the Use of the GeneSwitch Gal4 System to Knock-Down Genes in Drosophila melanogaster. *PLOS ONE*, 11(8), p.e0161817. doi:https://doi.org/10.1371/journal.pone.0161817.

Sellier, C., Campanari, M., Julie Corbier, C., Gaucherot, A., Kolb-Cheynel, I., Oulad-Abdelghani, M., Ruffenach, F., Page, A., Ciura, S., Kabashi, E. and Charlet-Berguerand, N. (2016). Loss of C9 ORF 72 impairs autophagy and synergizes with polyQ Ataxin-2 to induce motor neuron dysfunction and cell death. *The EMBO Journal*, 35(12), pp.1276–1297. doi:https://doi.org/10.15252/embj.201593350.

Shadfar, S., Brocardo, M. and Atkin, J.D. (2022). The Complex Mechanisms by Which Neurons Die Following DNA Damage in Neurodegenerative Diseases. *International Journal of Molecular Sciences*, 23(5), p.2484. doi:https://doi.org/10.3390/ijms23052484.

Sharpe, J.L., Harper, N.S., Garner, D.R. and West, R.J.H. (2021). Modeling C9orf72-Related Frontotemporal Dementia and Amyotrophic Lateral Sclerosis in Drosophila. *Frontiers in Cellular Neuroscience*, 15. doi:https://doi.org/10.3389/fncel.2021.770937.

Shi, Y., Lin, S., Staats, K.A., Li, Y., Chang, W.-H., Hung, S.-T., Hendricks, E., Linares, G.R., Wang, Y., Son, E.Y., Wen, X., Kisler, K., Wilkinson, B., Menendez, L., Sugawara, T., Woolwine, P., Huang, M., Cowan, M.J., Ge, B. and Koutsodendris, N. (2018). Haploinsufficiency leads to

neurodegeneration in C9ORF72 ALS/FTD human induced motor neurons. *Nature Medicine*, [online] 24(3), pp.313–325. doi:https://doi.org/10.1038/nm.4490.

Shibata, A. and Jeggo, P.A. (2021). ATM's Role in the Repair of DNA Double-Strand Breaks. *Genes*, 12(9), p.1370. doi:https://doi.org/10.3390/genes12091370.

Sieben, A., Van Langenhove, T., Engelborghs, S., Martin, J.-J., Boon, P., Cras, P., De Deyn, P.-P., Santens, P., Van Broeckhoven, C. and Cruts, M. (2012). The genetics and neuropathology of frontotemporal lobar degeneration. *Acta Neuropathologica*, 124(3), pp.353–372. doi:https://doi.org/10.1007/s00401-012-1029-x.

Simpson, J.E., Ince, P.G., Matthews, F.E., Shaw, P.J., Heath, P.R., Brayne, C., Garwood, C., Higginbottom, A. and Wharton, S.B. (2015). A neuronal DNA damage response is detected at the earliest stages of Alzheimer's neuropathology and correlates with cognitive impairment in the Medical Research Council's Cognitive Function and Ageing Study ageing brain cohort. *Neuropathology and Applied Neurobiology*, 41(4), pp.483–496. doi:https://doi.org/10.1111/nan.12202.

Smeyers, J., Banchi, E.-G. and Latouche, M. (2021). C9ORF72: What It Is, What It Does, and Why It Matters. *Frontiers in Cellular Neuroscience*, 15. doi:https://doi.org/10.3389/fncel.2021.661447.

Tao, Z., Wang, H., Xia, Q., Li, K., Li, K., Jiang, X., Xu, G., Wang, G. and Ying, Z. (2015). Nucleolar stress and impaired stress granule formation contribute to C9orf72 RAN translation-induced cytotoxicity. *Human Molecular Genetics*, 24(9), pp.2426–2441. doi:https://doi.org/10.1093/hmg/ddv005.

Taylor, M.J., Thompson, A.M., Alhajlah, S., Tuxworth, R.I. and Ahmed, Z. (2022). Inhibition of Chk2 promotes neuroprotection, axon regeneration, and functional recovery after CNS injury. *Science Advances*, 8(37). doi:https://doi.org/10.1126/sciadv.abq2611.

Taylor, M.J. and Tuxworth, R.I. (2019). Continuous tracking of startled Drosophila as an alternative to the negative geotaxis climbing assay. *Journal of Neurogenetics*, 33(3), pp.190–198. doi:https://doi.org/10.1080/01677063.2019.1634065.

Tuxworth, R.I., Taylor, M.J., Martin Anduaga, A., Hussien-Ali, A., Chatzimatthaiou, S., Longland, J., Thompson, A.M., Almutiri, S., Alifragis, P., Kyriacou, C.P., Kysela, B. and Ahmed, Z. (2019). Attenuating the DNA damage response to double-strand breaks restores function in models of CNS neurodegeneration. *Brain Communications*, [online] 1(1), p.fcz005. doi:https://doi.org/10.1093/braincomms/fcz005.

Walker, C., Herranz-Martin, S., Karyka, E., Liao, C., Lewis, K., Elsayed, W., Lukashchuk, V., Chiang, S.-C., Ray, S., Mulcahy, P.J., Jurga, M., Tsagakis, I., Iannitti, T., Chandran, J., Coldicott, I., De Vos, K.J., Hassan, M.K., Higginbottom, A., Shaw, P.J. and Hautbergue, G.M. (2017). C9orf72 expansion disrupts ATM-mediated chromosomal break repair. *Nature Neuroscience*, 20(9), pp.1225–1235. doi:https://doi.org/10.1038/nn.4604.

Wang, Y., Zhang, N., Zhang, L., Li, R., Fu, W., Ma, K., Li, X., Wang, L., Wang, J., Zhang, H., Gu, W., Zhu, W.-G. and Zhao, Y. (2016). Autophagy Regulates Chromatin Ubiquitination in DNA Damage Response through Elimination of SQSTM1/p62. *Molecular Cell*, 63(1), pp.34–48. doi:https://doi.org/10.1016/j.molcel.2016.05.027.

Webster, C.P., Smith, E.F., Bauer, C.S., Moller, A., Hautbergue, G.M., Ferraiuolo, L., Myszczynska, M.A., Higginbottom, A., Walsh, M.J., Whitworth, A.J., Kaspar, B.K., Meyer, K., Shaw, P.J., Grierson, A.J. and De Vos, K.J. (2016). The C9orf72 protein interacts with Rab1a and the ULK 1 complex to regulate initiation of autophagy. *The EMBO Journal*, 35(15), pp.1656–1676. doi:https://doi.org/10.15252/embj.201694401.

Westergard, T., Jensen, Brigid K., Wen, X., Cai, J., Kropf, E., Iacovitti, L., Pasinelli, P. and Trotti, D. (2016). Cell-to-Cell Transmission of Dipeptide Repeat Proteins Linked to C9orf72 - ALS/FTD. *Cell Reports*, 17(3), pp.645–652. doi:https://doi.org/10.1016/j.celrep.2016.09.032.

Xu, W. and Xu, J. (2018). C9orf72 Dipeptide Repeats Cause Selective Neurodegeneration and Cell-Autonomous Excitotoxicity in Drosophila Glutamatergic Neurons. *The Journal of Neuroscience*, 38(35), pp.7741–7752. doi:https://doi.org/10.1523/jneurosci.0908-18.2018.

Yoshida, S., Mulder, D.W., Kurland, L.T., Chu, C.-P. and Okazaki, H. (1986). Follow-Up Study on Amyotrophic Lateral Sclerosis in Rochester, Minn., 1925 through 1984. *Neuroepidemiology*, 5(2), pp.61–70. doi:https://doi.org/10.1159/000110815.

Zannini, L., Delia, D. and Buscemi, G. (2014). CHK2 kinase in the DNA damage response and beyond. *Journal of Molecular Cell Biology*, 6(6), pp.442–457. doi:https://doi.org/10.1093/jmcb/mju045.

Zhang, Y.-J., Jansen-West, K., Xu, Y.-F., Gendron, T.F., Bieniek, K.F., Lin, W.-L., Sasaguri, H., Caulfield, T., Hubbard, J., Daughrity, L., Chew, J., Belzil, V.V., Prudencio, M., Stankowski, J.N., Castanedes-Casey, M., Whitelaw, E., Ash, P.E.A., DeTure, M., Rademakers, R. and Boylan, K.B. (2014). Aggregation-prone c9FTD/ALS poly(GA) RAN-translated proteins cause neurotoxicity by inducing ER stress. *Acta Neuropathologica*, [online] 128(4), pp.505–524. doi:https://doi.org/10.1007/s00401-014-1336-5.

Zhu, L.-S., Wang, D.-Q., Cui, K., Liu, D. and Zhu, L.-Q. (2019). Emerging Perspectives on DNA Double-strand Breaks in Neurodegenerative Diseases. *Current Neuropharmacology*, [online] 17(12), pp.1146–1157. doi:https://doi.org/10.2174/1570159X17666190726115623.